Manuscript
Preprint

Marine biogenic emissions of benzene and toluene and their contribution to secondary organic aerosols over the polar oceans

Short title: Marine benzene and toluene emission enhance aerosol

Authors

Charel Wohl[1,2*], Qinyi Li[3], Carlos A. Cuevas[3], Rafael P. Fernandez[4], Mingxi Yang[2], Alfonso Saiz-Lopez[3], Rafel Simó[1]

Affiliations

[1]Department of Marine Biogeochemistry, Institut de Ciències del Mar, ICM-CSIC, Barcelona, 08003, Catalonia, Spain.

[2] Plymouth Marine Laboratory, Plymouth, PL1 3DH, United Kingdom.

[3]Department of Atmospheric Chemistry and Climate, Institute of Physical Chemistry Rocasolano, IQFR-CSIC, Madrid, 28006, Spain.

[4]Institute for Interdisciplinary Science (ICB), National Research Council (CONICET), FCEN-UNCuyo, Mendoza, 5500, Argentina.

First and corresponding author: Charel Wohl (cwohl@icm.csic.es)

Submitted for preprint Dec 2022

Abstract

Natural processes in the polar oceans lead to emission of a variety of reactive gases contributing to atmospheric chemistry and aerosol formation. The identity and air–sea fluxes of most of these gases are poorly characterized, bringing uncertainty to the assessment of pre-industrial aerosol sources. Here we present seawater and atmospheric measurements of benzene and toluene in the open Southern Ocean and the Arctic marginal ice zone. Our data suggest a marine biogenic source for these two compounds, which have typically been associated with anthropogenic pollution. Calculated average emission fluxes were 0.024 and 0.037 μmol m^{-2} d^{-1} for benzene and toluene, respectively. Including the observed emissions in a chemistry–climate model increased secondary organic aerosol mass concentrations only by 0.1–1.2 % over the Arctic but by 7.7–77.3 % over the Southern Ocean far from continental sources. Climate models must consider the hitherto overlooked emissions of biogenic benzene and toluene from pristine oceanic regions.

Teaser

Biogenic benzene and toluene emissions from the polar oceans enhance atmospheric secondary organic aerosol mass.

Introduction

The microbiota of the world's oceans produce a plethora of organic gases leading to ocean emissions (*1–4*). Such emissions are particularly important for atmospheric chemistry in the polar regions which are relatively pristine and far away from terrestrial sources (*5*, *6*). Among organic gases, non-methane hydrocarbons can act as a sink for OH in marine air (*7*, *8*) and can contribute substantially to aerosol (*9–11*) as well as new particle formation (*5*). Accurately quantifying natural marine aerosol particularly in the polar regions is crucial to estimate aerosol climate forcing (*9*, *12*, *13*), especially since secondary organic aerosols (SOA) have been suggested to exert a strong effect on cloud formation (*14*). The term SOA refers to the organic fraction of aerosol derived from atmospherically oxidised organic precursor compounds. Global models currently hugely underestimate marine aerosol (*15*, *16*) and parameters such as aerosol optical depth (*17*) or aerosol concentrations (*18*) in regions where anthropogenic influence is lowest. Studying the pristine ocean atmosphere allows understanding and setting of the pre-industrial (i.e. pristine) baseline of SOA precursors, which is critical for modelling assessments of anthropogenic forcing (*19*, *20*).

Solving the aerosol underestimate by models requires to accurately quantify the total marine emissions of aerosol-forming organic gases and predict their paths to SOA formation. Revealing the identity of these gases is crucial as well because the efficiency with which organic gases are oxidised into SOA components varies largely across compounds. Chamber studies generally show that the aerosol forming yield of to date well-studied marine biological gases is rather low; 2-7 % for dimethylsulfide (DMS) (*21*), around 2 % for isoprene (*22*) and 1-68 % for monoterpenes depending on the species (*23*). In contrast, the SOA forming yield is much higher for benzene (36 %) and toluene (30 %), especially in low-NO_x regimes (*24*). Benzene and toluene are traditionally associated with anthropogenic emissions - the largest sources being coal or petroleum combustion, crude oil processing and solvent use followed by biomass burning (*25*). Their largest sink in the atmosphere is the oxidation by rapid reaction with OH (*25*). Benzene and toluene have been measured in the atmosphere of the remote polar and temperate oceans (*26*, *27*), suggesting that they are common and pervasive organic species in the atmosphere. It is unclear whether the oceans act as a source or a sink of benzene and toluene, especially in natural environments. If occurring, sea-to-air fluxes (ocean source) of benzene and toluene to the remote marine atmosphere would be particularly important owing to their high SOA formation potential and rapid reaction rate with OH. Guo et al. (*28*) found traces of aromatic (i.e. benzene and toluene) oxidation products in marine organic aerosol in the northwest Pacific.

Recently, Rocco et al. (*29*) suggested a phytoplankton source of benzene and toluene in the surface ocean. They used mesocosm and phytoplankton culture experiments to show that phytoplankton species produce benzene and toluene at variable rates. Misztal et al. (*30*) also used mesocosm experiments to suggest a diurnally varying source of toluene from the coccolithophore microalga *Emiliania huxleyi*. There also exists some evidence for toluene production by the coral microalgal symbionts *Symbiodiniaceae* and two members of its core bacterial microbiome (*31*). Toluene has been found to be produced by 20 bacterial genera (*32*) and by bacteria isolated from surface seawater in Antarctica (*33*). This set of evidence suggests that both phytoplankton and marine bacteria play a role in producing toluene in seawater. While experiments show that benzene and toluene can be produced by marine biota, in situ measurements are needed to quantify the magnitude of their air–sea flux and the atmospheric importance thereof.

Air–sea benzene and toluene fluxes can be estimated using the bulk two-layer model (*34*), which requires concentrations of benzene and toluene in the surface ocean and lower atmosphere. Ambient air measurements of benzene and toluene have become very common, especially since the introduction of Proton Transfer Reaction-Mass Spectrometers (*26*, *27*, *35*, *36*). However, to our knowledge, there have been very few reported concentrations of benzene and toluene in seawater. Only Sauer (*37*) reported 64–192 pmol dm^{-3} benzene and 32–108 pmol dm^{-3} toluene in unpolluted surface seawater of the gulf of Mexico. There are no measurements alongside biological proxies in the water column at different depths, which could give important clues to their sources and sinks in the ocean. With anthropogenic activity likely to increase in the changing polar regions, seawater measurements of benzene and toluene are timely and represent a useful benchmark. Rocco et al. (*29*) performed benzene and toluene flux observations in the Southern Ocean, however their flux estimates were restricted to a few episodes and relied upon the indirect nocturnal accumulation method (*29*, *38*). Such observations of episodic outgassing from the ocean are not sufficient to ascertain if the ocean is a pervasive net source of benzene and toluene, given the variety of other sources to the global atmosphere.

Here we present benzene and toluene measurements in seawater and ambient air in the open Southern Ocean and the Arctic marginal sea ice zone. Our novel seawater measurements from both polar oceans include high-resolution surface underway measurements and depth profiles, which are compared to chlorophyll fluorescence and density profiles to explore the possible marine sources of benzene and toluene. The high-resolution measurements at both sides of the air–sea interface are used to calculate the oceanic saturation and the net fluxes at high resolution using the two-layer bulk flux method. These oceanic emission fluxes are incorporated in a global chemistry–climate model, the Community Atmospheric Model with Chemistry (CAM-Chem (*39*)), to assess the atmospheric implications of ocean benzene and toluene outgassing over the polar oceans. We find that benzene and toluene emission fluxes significantly increase the modelled SOA, especially over the remote Southern Ocean.

Results

Southern Ocean observations

Depth Profiles

A total of 28 CTD (Conductivity/Temperature/Depth) stations were vertically profiled for benzene and toluene in the Southern Ocean. For the ease of visualisation and analysis, the CTD stations were classified by surface Chl *a* (Chlorophyll *a*) concentration; low Chl *a* 0–0.2 mg m^{-3}, medium Chl *a* 0.2–0.5 mg m^{-3} and high Chl *a* 0.5–1 mg m^{-3}. Higher Chl *a* concentrations are indicative of high phytoplankton activity. These thresholds were chosen as they corresponded to patterns in benzene and toluene depth profile distributions, and reflect the distribution of Chl *a* in the Southern Ocean (*40*). The highest surface concentration measured during the cruise was 1 mg m^{-3}. Grouped stations were averaged in depth bins to help tease out patterns (Figure 1). Cruise track with CTD sampling locations (Figure S1) and individual vertical profiles of benzene, toluene, Chl *a* and seawater density are shown in the supplement (Figure S2 and S3), while additional details regarding the Chl *a* data, analytical chemistry and measurement uncertainty are provided in the supplementary text.

The depth profiles reveal that benzene concentrations were generally higher in the top 75 m, along with elevated Chl *a* concentrations. The benzene profiles displayed concentrations of around 10 pmol dm^{-3} in the upper 200 m in low Chl

a casts, and on average around 20 pmol dm^{-3} and 30 pmol dm^{-3} in the upper 75 m in the medium and high Chl *a* casts, respectively. Chl *a* and benzene depth profiles showed remarkable co-variation with depth across Chl *a* regimes. Conversely, toluene concentrations were not always highest in the top 75 m, and their profile shape and mean concentrations did not always follow the distribution of Chl *a*. Yet, higher toluene concentrations near the surface were commonly observed in casts with high Chl *a*. The absence of a clear pattern with depth is probably due to toluene origin not only in phytoplankton but also in bacteria (*32*, *33*) which are not related to Chl *a*, as well as toluene's short lifetime (*41*, *42*) that prevents accumulation. These depth profiles support distinct biological sources of benzene and toluene in seawater.

Underway surface concentrations and flux estimates

Ambient air, underway surface seawater measurements and calculated air–sea fluxes of benzene and toluene are shown in Figure 2. Positive fluxes indicate oceanic outgassing, i.e. sea-to-air flux. Interruptions in the air measurements were largely due to ship stack contamination. Fluxes were computed in two ways, using either measured air mole fractions or interpolated air measurements. Both sets of fluxes are weighted by the number of data points to avoid bias in the reported cruise means.

Figure 2 shows that measurements from the 5 m discrete samples and the underway inlet compared well within measurement noise, which confirms that the ship's underway inlet did not contaminate our measurements. Mean underway surface seawater benzene and toluene concentrations were very similar (cruise mean ± standard deviation, benzene 17 ± 11 pmol dm^{-3}, toluene 17 ± 9 pmol dm^{-3}) and both displayed a large range: for benzene from the limit of detection (LOD) to 73 pmol dm^{-3}, and for toluene from 5 pmol dm^{-3} to 72 pmol dm^{-3}. Previous mesocosm experiments (*30*) have suggested a diurnally varying source of benzene and toluene in the ocean (*43*). However, diurnal variability is not obvious in our data (Figure S4). Instead, we observed sporadic episodes of very high seawater benzene and toluene concentrations on top of relatively constant background levels. This is a very characteristic distribution for compounds produced by biological processes, as is the case for example for DMS (*2*) and isoprene (*44*). The median seawater concentration of benzene (13 pmol dm^{-3}) and toluene (15 pmol dm^{-3}) were lower than the mean which illustrates a greater skewness for benzene than for toluene. Despite similar mean concentrations, benzene and toluene usually did not peak at the same time. For example, benzene concentrations in seawater were very high in an area of high Chl *a* concentration sampled around 13/3/19, while toluene concentrations in this area were near the cruise average. Consequently, benzene and toluene underway seawater concentrations correlated significantly, but weakly during this cruise track ($R = 0.07$; $P<0.001$; $N=885$), suggesting different source and sink strengths for the two compounds. Benzene correlated significantly but weakly with Chl *a* ($R=0.34$; $P<0.001$; $N=859$) and strongly with DMS ($R=0.70$; $P<0.001$; $N=868$), while toluene did not correlate with either. The correlation of benzene with Chl *a* is consistent with the findings from the depth profiles. Toluene did correlate weakly with isoprene ($R=0.08$; $P<0.001$; $N=825$). Overall, significant correlations with a phytoplankton proxy (Chl *a*) and/or other biogenic trace gases (DMS, isoprene) support a biological source for benzene and toluene in seawater.

Cruise mean ambient air benzene mole fractions were lower than typically observed at terrestrial sites (benzene 14 ± 17 pmol mol^{-1}) (*25*), while toluene mole fractions were essentially near zero and below the limit of detection for most of the cruise track. Such low ambient air mole fractions over the Southern Ocean are similar to observations by Guérette

et al. (*36*) and Rocco et al. (*29*), who also observed less than 20 pmol mol^{-1} benzene and toluene on average over the Southern Ocean. Our observations of higher concentrations of benzene compared to toluene are likely related to the faster reaction with OH and shorter atmospheric lifetime of toluene (*24*). Low and homogenous mole fractions as well as the absence of a significant correlation (R=0.01; P=0.1; N=237) between benzene and toluene mole fractions suggest that the concentrations measured during this cruise were largely produced by local and diffuse sources, e.g. many episodes of oceanic outgassing rapidly mixed by winds, and not by transport of polluted air masses.

During this cruise, the fluxes of benzene and toluene were almost always from the ocean to the atmosphere. The cruise mean saturation (an indication of the thermodynamic forcing and direction of the flux, here a saturation above 100 % indicates outgassing) was 192 ± 121 % for benzene and 173 ± 106 % for toluene, while the cruise mean fluxes were 0.023 ± 0.030 µmol m^{-2} d^{-1} for benzene and 0.039 ± 0.036 µmol m^{-2} d^{-1} for toluene. There was a large range in the benzene and toluene fluxes, with a maximum of 0.358 µmol m^{-2} d^{-1} for benzene and 0.158 µmol m^{-2} d^{-1} for toluene. To put these emissions into context, the mean benzene and toluene fluxes out of the ocean were comparable (i.e. within 0.007 µmol m^{-2} d^{-1}) to the mean isoprene flux measured during the same cruise (*45*). These benzene and toluene fluxes are also in the same order of magnitude (i.e. within 0.012 µmol m^{-2} d^{-1}) as mean monoterpene fluxes reported from the northwest Atlantic (*46*). This illustrates that, on a molar per area basis, benzene and toluene fluxes rival emissions by other hitherto better known marine biological gases. We observe lower median fluxes of benzene (0.012 µmol m^{-2} d^{-1}) and toluene (0.034 µmol m^{-2} d^{-1}) compared to the mean, which illustrates skewedness of the data distribution and larger outgassing events influencing the mean. Rocco et al. (*29*) calculated emissions of 1.3 µmol m^{-2} d^{-1} (= 1.2 ng m^{-2} s^{-1}) benzene and 3.5 µmol m^{-2} d^{-1} (= 3.7 ng m^{-2} s^{-1}) toluene. This is more than sixty times larger than our mean and 3 (benzene) and 22 (toluene) times larger than our highest outgassing fluxes. It is worth noting that the flux estimates from Rocco et al. (*29*) are based on three nights only and were calculated using the nocturnal accumulation method. This method assumes that night-time losses from reaction with OH are negligible and that ocean emissions accumulate overnight in a well-mixed marine boundary layer. Any night-time increase (which have only been detected reliably for three nights in their works (*29*)) is assumed to be due to ocean outgassing (which is not necessarily a given for atmospheric benzene and toluene due to the existence of continental sources of these compounds). This method can only be applied to nights when there was substantial outgassing, which could lead to an overestimate of the true mean flux. The nocturnal accumulation method has thus far only been used for DMS (*38*) and methanethiol (*47*), and only validated for DMS, two gases that are well known to be consistently supersaturated in the ocean and have essentially only marine sources.

Canadian Arctic observations

Depth profiles

A total of 24 depth profiles were measured during this deployment. In the marginal ice zone in summer and spring, the sea ice cover controls the biogeochemistry and the physical structure of the water column, including the distribution of Chl *a* and density (*48*) as well as bacterial activity (*49*). Thus, exactly as in Wohl et al. (*50*), vertical profiles were classified by sea ice cover (SIC) at the time of sampling (Figure 3). Details of the Chl *a* measurements, the analytical chemistry, measurement noise and the cruise track are presented in the supplementary text.

The individual depth profiles of benzene and toluene showed less identifiable patterns than those in the Southern Ocean (Figure S5 and S6). Hence, we use depth bin averaging to make the trends visually clearer (Figure 3). Within the 75 to 90 % SIC bin (near-full sea ice cover), benzene and toluene concentrations gradually decreased from the surface to 20–30 m. At partial sea ice cover (20–50 % SIC), benzene and toluene were mixed more homogenously within the 40 m near the surface. In ice-free conditions (0 % SIC), subsurface peaks in benzene and toluene occurred which were often situated around a subsurface peak in Chl *a* concentration. In the Arctic, a substantial amount of biological activity occurs below the surface at this Chl *a* peak (*51*). Thus, subsurface peaks of benzene and toluene co-located with Chl *a* support a biological source. Other biogenic gases, such as DMS and isoprene also displayed higher concentrations at the depth of peak Chl *a* concentration compared to 5 m below the surface (*50*). About 20 % of the stations displayed higher concentrations at 30 cm than at 2 m. The concentration increase often coincided with lower seawater density (Figure S5 and S6) and suggests fine scale vertical variability in the processes controlling concentrations of benzene and toluene, similar to other biogenic gases during this cruise (*50*). Overall, these measurements support distinct biological sources for benzene and toluene in the Arctic Ocean related to Chl *a*, though the precise factors controlling their distribution are far from clear.

Underway concentrations and flux estimates

Underway concentration measurements and air–sea flux estimates of benzene and toluene in the Canadian Arctic marginal sea ice zone during boreal summer are shown in Figure 4. Underway and 5 m discrete measurements agreed well within measurement uncertainty. Mean seawater concentrations were two times for benzene (37 ± 24 pmol dm^{-3}) and three times for toluene (46 ± 24 pmol dm^{-3}) higher than those in the Southern Ocean cruise. This could be due to either higher biological activity (it was earlier in the productive season) or larger anthropogenic influence and thus higher contribution of anthropogenic benzene and toluene to observed seawater concentrations. Due to the short residence times of benzene and toluene in unpolluted seawater (less than 1 day (*42*)), we expect any anthropogenic influence to be due to local sources. Similar to the cruise in the Southern Ocean, concentrations displayed a wide range from near the LOD to up to 131 pmol dm^{-3} and 139 pmol dm^{-3} for benzene and toluene respectively. Also, similar to the Southern Ocean, the median benzene concentration (30 pmol dm^{-3}) was lower than the mean, though in contrast, toluene median concentration was the same as the mean. Skewed data distribution of peak concentrations amongst an apparently constant background is typical for biologically produced compounds. There was no significant correlation between Chl *a* and benzene ($0<R<0.01$; $P=0.53$; $N=219$) or toluene ($0<R<0.02$; $P=0.058$; $N=223$). The depth profiles suggest that the lack of a correlation with Chl *a* is probably because much of the biological activity and production of benzene and toluene occurred at depths below 5 m while the underway measurements were taken at 3–4 m. Benzene and toluene also did not correlate with isoprene or sea ice cover. In contrast to the Southern Ocean, here there was a weak yet significant correlation between benzene and toluene ($R=0.21$; $P<0.001$; $N=245$). Both benzene and toluene correlated positively with seawater DMS ($R=0.18$; $P<0.001$; $N=239$; and $R=0.10$; $P<0.001$; $N=239$, respectively). Overall, the underway surface ocean measurements further support that at least part of the benzene and toluene had a biological origin, potentially with contributions of local pollution.

Atmospheric mole fractions of benzene and toluene were not measured on the Arctic cruise. To estimate air–sea flux and mean saturation, we used previous air measurements of these compounds at a similar location (western Canadian Arctic) and similar time of year (August–September) by Sjostedt et al. (*35*) (13 pmol mol^{-1} benzene and 4 pmol mol^{-1}

toluene). This is comparable to a more recent study by Pernov et al. (*52*), who measured 27 pmol mol^{-1} benzene near the coast in Northeast Greenland. Using the measurements from Sjostedt et al. (*35*), saturation and fluxes were calculated and are presented in Figure 4. The ocean was highly supersaturated in benzene (610 ± 386 %) and toluene (2335 ± 1175 %) and thus uncertainty in the air mole fractions should not affect the flux very much, similarly to isoprene (*53*). In the supplement Table S1, we show that alternative fluxes and saturations calculated with air mole fractions in the Arctic modelled by Cabrera-Perez et al. (*25*), which are higher than those of Sjostedt et al. (*35*). The results illustrate that the choice of the air mole fraction does not change the conclusion that the Arctic ocean was consistently outgassing benzene and toluene. Cruise mean fluxes were 0.023 ± 0.028 µmol m^{-2} d^{-1} for benzene and 0.034 ± 0.041 µmol m^{-2} d^{-1} for toluene. Surface ocean concentrations and supersaturations were much higher in the Arctic than in the Southern Ocean. However, the mean fluxes from the two cruises were similar. This is due to the lower estimated air–sea transfer velocities in the Arctic, which resulted from lower wind speeds as well as sea ice acting as a barrier to air–sea exchange in our calculation. Benzene and toluene fluxes displayed a lower median than mean flux (benzene median flux 0.014 µmol m^{-2} d^{-1}, toluene median flux 0.020 µmol m^{-2} d^{-1}). Therefore, reported mean fluxes were influenced by strong outgassing episodes that coincided with above-average seawater concentrations, high winds and low sea ice cover, e.g. on 31/07 and 01/08. The highest hourly measured outgassing flux was 0.158 µmol m^{-2} d^{-1} for benzene and 0.268 µmol m^{-2} d^{-1} for toluene. Similar to the cruise in the Southern Ocean, the mean emissions of benzene and toluene from this cruise in the Arctic marginal ice zone are comparable (within 0.024 µmol m^{-2} d^{-1}) to the isoprene flux from the same deployment (*50*).

Even though our flux calculations were not very sensitive to a range of realistic atmospheric mole fractions, could increased anthropogenic activity in the Arctic reverse the direction of the benzene and toluene fluxes? If we assumed around 50 pmol mol^{-1} benzene and 30 pmol mol^{-1} toluene in the marine atmosphere as modelled for the busy shipping corridors of the North Atlantic and North Pacific (*25*), the estimated mean saturations would be 159 and 311 %, and the mean fluxes would be 0.011 and 0.026 µmol m^{-2} d^{-1} for benzene and toluene, respectively. Assuming that seawater concentrations remain unaffected by shipping, this suggests that even if anthropogenic activity largely increased in the Arctic, benzene and toluene are likely still to be emitted to the atmosphere from the ocean. Ambient air mole fractions above 79 pmol mol^{-1} benzene and 91 pmol mol^{-1} toluene would be required to lead to ocean uptake in the Arctic summer (considering the seawater solubilities and the mean benzene and toluene seawater concentrations from this cruise). Such high atmospheric mole fractions are only predicted for densely populated areas (*25*).

Atmospheric effects of oceanic benzene and toluene emissions

The effects of these ocean emissions of biogenic benzene and toluene on atmospheric chemistry were assessed using a global chemistry–climate model (CAM-Chem (*39*)). Table 1 shows simulated atmospheric mole fractions of benzene, toluene, and OH in the three simulation cases (noBT, avgBT, and maxBT; Table S2), along with the changes between cases. Adding our mean measured benzene and toluene ocean flux to the model increased benzene and toluene atmospheric mole fractions by 1.7–3.2 pmol mol^{-1} with respect to the noBT case where there is no oceanic efflux and polar airborne benzene and toluene result from long-distance transport alone. Due to the low simulated background concentrations, the contribution of oceanic emissions represents a 12 % (benzene) and 100 % (toluene) increase in the Arctic, and as much as a 3- (benzene) and 30- (toluene) fold increase in the Southern Ocean. The model results compare well with our Southern Ocean observations of 14 ± 17 pmol mol^{-1} benzene, while toluene mole fractions were below

the LOD. The air mole fractions modelled for the Arctic in the noBT case were within 7 pmol mol^{-1} of the ones used to compute the flux and saturations, which is reassuring.

Despite their rapid reaction with OH, due to their low atmospheric concentrations the oceanic benzene and toluene emissions do not significantly impact on model OH concentrations, which only decreased by less than 0.02 % even when the cruise-maximum emissions were considered. Thus, OH sinks other than benzene and toluene prevail (*7*, *8*). A better assessment of the overall impact of benzene and toluene on OH would require a more complete emission inventory of aromatics in the model. For example, using a comprehensive list of annual anthropogenic and biomass burning emissions, Taraborrelli et al. (*54*) found that aromatics decrease model OH concentrations over the ocean by 2–5 %. However, the inclusion of our mean emission fluxes increased the amount of SOA that is formed from benzene and toluene by ~1 and 6.3 % in the Arctic, respectively. In the Southern Ocean, the increases in benzene and toluene-derived SOA due to including oceanic emissions are 12.8 % and 139.8 % (Figure 5). Note that the simulated background SOA mass concentrations in the Arctic are more than 25 times those in the Southern Ocean. The majority of benzene and toluene in the Arctic that forms SOA comes from terrestrial emissions, which dwarf the oceanic benzene and toluene emissions. As such, adding our mean and maximum calculated Arctic ocean emission flux to the CAM-Chem model increases SOA concentration by 0.1 and 1.2 % respectively. In contrast, over the pristine Southern Ocean, farther away from continental influence, the impact of oceanic benzene and toluene emission on SOA is far greater: our cruise-average fluxes increased total SOA mass concentration by 7.7 % and total organic (primary + secondary) aerosol by 6.7 % (Figure 9). Therefore, ocean biological emissions of benzene and toluene probably contribute to the observed summertime increase in total organic aerosol and SOA over the Southern Ocean (*15*, *55*). In comparison, Arnold et al. (*22*) estimated that ocean isoprene emissions contribute only 0.2 to 1.3 % to SOA and organic aerosol mass concentrations over the Southern Ocean. Thus, marine benzene and toluene can be more important SOA (and, by extension, organic aerosol) precursors than marine isoprene, at least in the Southern Ocean. Running the model with the cruise-maximum Southern Ocean fluxes instead of the cruise-mean emission fluxes, the mass concentration of benzene and toluene derived SOA increased by 298.0 and 748.2 %, respectively (Figure 5). This results in an increase in total SOA of 77.3 % and an increase of the total organic aerosol by 67.4 % and indicates that episodes of high ocean emissions of benzene and toluene may have a large local impact on SOA.

The model also estimated the concentration of non-sea-salt sulfate aerosol (derived from oceanic DMS emissions and anthropogenic SO_2 transport) to be 0.323 μg m^{-3} in the Arctic and 0.059 μg m^{-3} in the Antarctic in all model runs. Comparison with SOA mass concentrations reveals that, despite the addition of marine benzene and toluene emissions to the model, sulfate dominates the secondary aerosol composition in both polar regions. Indeed, the calculated emission fluxes of DMS were 20-fold those of benzene and toluene during both cruises (*45*, *50*). Consequently, cruise-mean and cruise-maximum benzene and toluene emissions increased total secondary aerosol (SOA + non-sea-salt sulfate aerosol) by less than 2 % in all model runs and for both polar oceans. Even though benzene and toluene do not contribute as much to aerosol mass compared to DMS, they are a source of highly oxygenated organic molecules (*56*) that condense onto existing particles and contribute to aerosol growth (*57*). Oxidised aromatics alter particle properties and may help explain the lower-than-expected particle hygroscopicity over the Southern Ocean (*58*).

Overall, our modelling results show that ocean benzene and toluene emissions enhance SOA in the polar regions, especially over the pristine Southern Ocean, where episodic localized emissions have a disproportionate contribution to SOA mass.

Discussion

In this manuscript, we present seawater concentrations and atmospheric measurements of benzene and toluene from two cruises in the polar oceans. Benzene and toluene concentrations were measured in surface seawater and in a large number of depth profiles. This unique combination of measurements points towards a biological source for these two compounds previously thought to be predominantly released to the environment from anthropogenic activity. Concurrent high-resolution measurements in the surface seawater and the overlying atmosphere showed that both the Arctic and the Southern Ocean were highly supersaturated in benzene and toluene, and their emission fluxes rivalled those of other atmospherically relevant marine trace gases, such as isoprene or monoterpenes. Implementing these emission fluxes in a global chemistry–climate model, we estimated that ocean-leaving benzene and toluene made significant contributions to SOA mass concentration in the polar regions, with the largest effect over the pristine Southern Ocean (7.7 % increase in SOA as the average effect, and up to 77.3 % increase using the highest measured emission flux). Even though a note of caution must be sound on the limited spatial and temporal coverage of our cruises, these results indicate that the inclusion of natural oceanic emissions of benzene and toluene in global models will help to reduce the current underestimates in naturally produced total (*16*) and cloud-forming (*18*) aerosols over the oceans. Our findings also call for expanding both the measurements and the model representations of other, hitherto overlooked, gas precursors of SOA in the marine atmosphere.

We note that our modelling focuses on aerosol mass concentrations, whereas benzene and toluene emissions are likely to also impact aerosol hygroscopicity and thus the ability of aerosol to form clouds. Further studies that track the fate of these aromatic compounds on marine aerosols should be conducted if we are to reduce the uncertainty of climate predictions due to aerosol direct and indirect forcing (*14*). Overall, this work provides new insights on the connections between polar ocean biological processes and climate through the identification and quantification of new natural sources of marine aerosol. This will help to define the pre-industrial baseline in aerosol precursors and aid modelling assessments of the subsequent anthropogenic forcing (*19*, *20*).

Materials and Methods

Benzene and Toluene air and seawater measurements and fluxes

Benzene and toluene were measured on both cruises using a Proton Transfer Reaction Mass Spectrometer (Ionicon PTR-MS, high sensitivity with a quadrupole) coupled to a Segmented Flow Coil Equilibrator (SFCE). Details on the installation on board for each cruise are provided elsewhere (*45*, *50*, *59*). Briefly, the PTR-MS and the SFCE were installed on the ship in a laboratory near an underway water tap. During the cruise in the Southern Ocean, an air pump was used to rapidly draw ambient air from about 16 m above sea level to the laboratory, where the PTR-MS sub-sampled from a tee piece upstream of the pump. Solenoids were used to set up an hourly cycle of measuring SFCE headspace, ambient air and ambient air passed through a Pt-catalyst, which acts as a blank measurement. During the

Arctic cruise, SFCE headspace was sampled continuously. The SFCE sampled seawater from the underway water supply (Southern Ocean cruise: 4–7 m depth, Arctic cruise: 3–4 m depth) via an overflowing glass bottle. To make vertical profile measurements, waters were collected from CTD rosette into 900 cm^3 glass bottles and sampled with the SFCE.

In the PTR-MS, m/Q 79 and m/Q 93 were taken to be benzene and toluene respectively in accordance with previous mass assignments (*52*, *60*). During both cruises, the PTR-MS was calibrated using a multi-component gas standard containing benzene and toluene (supplementary text). During the Southern Ocean cruise, the hourly measurement of outside air scrubbed by the Pt-catalyst was used as a blank for the benzene air measurements, while daily measurements of zero air from a gas standard were used as a blank for toluene air measurements. The air measurements were carefully filtered for ship stack contamination as laid out in Wohl et al. (*45*).

Dissolved concentrations of benzene and toluene were computed based on solubility from a set of equations presented in Wohl et al. (*59*). A detailed discussion of the measurement background and the limit of detection and measurement uncertainty are provided in the supplementary text.

Our specific equations to calculate air–sea fluxes are laid out in detail in Wohl et al. (*45*). Here we provide a brief recap and additional details specific to benzene and toluene. Air–sea fluxes are calculated using the Liss and Slater (*61*) two-layer framework. Benzene and toluene fluxes are computed using the waterside transfer velocity from Nightingale et al. (*62*) and the airside transfer velocity from Yang et al. (*63*). Freshwater solubilities (dimensionless water over air) for benzene and toluene listed in Wohl et al. (*59*) were converted to seawater solubilities at the temperature of ambient seawater as described in Johnson (*64*). The Schmidt number for toluene was calculated using the supplementary R code from Johnson (*64*). The Schmidt number for benzene was calculated from the diffusivity of benzene and assuming the same temperature dependence as toluene. Saturations (see equation 1 in Wohl et al. (*45*)) were not computed if the hourly air mole fraction is near or below zero (defined as less than one measurement noise) to avoid unrealistic values. Calculated fluxes were scaled linearly to the open water fraction as recommended by Prytherch et al. (*65*). To do this, the underway SIC was used as derived from AMSR2 satellite.

DMS and isoprene concentrations and fluxes were also measured during both deployments. Their concentrations are shown elsewhere (*45*, *50*) and used here to test for correlations with benzene and toluene.

CAM-Chem simulations

We used a global chemistry–climate model, the Community Atmosphere Model with Chemistry (CAM-Chem; Lamarque et al. (*39*) and Saiz-Lopez et al. (*66*)) to quantify the potential effects of the derived oceanic flux of benzene and toluene on atmospheric composition. CAM-Chem is designed to perform both, climate simulations (with online simulation of climate system) and simulations with specified dynamics (nudged to offline meteorology fields). The implementation of SOA formation embedded in CAM-Chem is described in Lamarque et al. (*39*) and Lack et al. (*67*). Briefly, the CAM-Chem model applies the 2-product parameterization (*68*) to simulate the SOA formation, considers SOA formations from the oxidation of VOCs (monoterpenes, isoprene, benzene, toluene, and xylene), and includes reactions with key oxidants (OH, O_3, NO_3). The formed quantity of SOA at each time step depends on the gas-phase

oxidation rate of VOCs (calculated in the gaseous chemistry module) and the production yield (estimated online based on the existing organic aerosol and the relative abundance of NO versus HO_2, the so-called high NO_x and low NO_x conditions (*69*). The produced SOA increases the total burden of organic aerosol, either via condensing onto the existing aerosol or forming new aerosols. Here we further update the model to include alkanes and alkenes as the additional SOA precursors following Mahmud and Barsanti (*70*) and to include Cl and Br atoms as the additional oxidants following Choi et al. (*71*) and Li et al. (*72*).

The CAM-Chem simulations were conducted in specified dynamic mode (nudged to GEOS5 meteorological data) so that we can isolate the chemical impacts of the additional oceanic emissions of benzene and toluene on the atmospheric levels of benzene, toluene, oxidants (OH), and SOA. The simulations were run from Jan 2017 to Dec 2019 and the results in the first 6 months were discarded as spin-up. For the anthropogenic and biomass burning sources of air pollutants, including NO_x, SO_2, CO, NH_3, VOCs (e.g. benzene, toluene and many others), we used the emission inventories compiled for the ongoing CMIP6 project (*73*). The terrestrial biological emissions of VOCs (e.g. isoprene, monoterpenes) are calculated online using MEGAN2 (*74*). It is worth mentioning that being a global chemistry-climate model, CAM-Chem includes the transport of terrestrial emissions of VOCs to the marine atmosphere. A climatology of oceanic emission of DMS, used in previous CESM simulations (e.g. Tilmes et al. (*75*) and Veres et al. (*76*)), is also included, which is the only oceanic emission of reactive gas considered in this model.

In total, we have conducted three simulation cases (Table S2), coined the noBT, avgBT, and maxBT cases. The noBT case contains no oceanic emissions of benzene and toluene; the avgBT case includes the average oceanic emission fluxes of benzene and toluene for both polar oceans (all oceanic regions > 60 ºN and < -55 ºS) taken from the cruise measurements; the maxBT case applies the maximum oceanic fluxes for the polar oceans (i.e. the highest hourly measured/calculated oceanic outgassing flux). The difference in the atmospheric compositions (benzene and toluene mole fractions, OH, and SOA) between avgBT and noBT cases represent the effects of the average oceanic flux of benzene and toluene in the atmosphere. The difference between maxBT and noBT illustrates the impact of the maximum fluxes. Note that all modelling results have been averaged by sampling CAM-Chem grid points at the exact location and time (month) of each cruise. By designing these cases, we attempt to capture the most probable effects of the additional oceanic aromatic emissions (noBT v.s. avgBT) as well as the possible range of such effects (noBT v.s. maxBT). The CAM-Chem simulation results are described in the section "Atmopsheric effects of oceanic benzene and toluene emissions".

References

1. L. J. Carpenter, S. D. Archer, R. Beale, Ocean-atmosphere trace gas exchange. *Chem. Soc. Rev.* **41**, 6473 (2012).
2. S. Hulswar, R. Simó, M. Galí, T. G. Bell, A. Lana, S. Inamdar, P. R. Halloran, G. Manville, A. S. Mahajan, Third Revision of the Global Surface Seawater Dimethyl Sulfide Climatology (DMS-Rev3). *Earth Syst. Sci. Data.* **14**, 2963–2987 (2022).
3. N. Tripathi, L. K. Sahu, A. Singh, R. Yadav, A. Patel, K. Patel, P. Meenu, Elevated Levels of Biogenic Nonmethane Hydrocarbons in the Marine Boundary Layer of the Arabian Sea During the Intermonsoon. *J. Geophys. Res. Atmos.* **125**, 20–30 (2020).
4. R. Uning, M. T. Latif, H. H. A. Hamid, M. S. Mohd Nadzir, M. F. Khan, S. Suratman, Sea-to-Air Fluxes of Isoprene and Monoterpenes in the Coastal Upwelling Region of

Peninsular Malaysia. *ACS Earth Sp. Chem.* **5**, 3429–3436 (2021).
5. D. B. Collins, J. Burkart, R. Y. W. Chang, M. Lizotte, A. Boivin-Rioux, M. Blais, E. L. Mungall, M. Boyer, V. E. Irish, G. Massé, D. Kunkel, J. É. Tremblay, T. Papakyriakou, A. K. Bertram, H. Bozem, M. Gosselin, M. Levasseur, J. P. D. Abbatt, Frequent ultrafine particle formation and growth in Canadian Arctic marine and coastal environments. *Atmos. Chem. Phys.* **17**, 13119–13138 (2017).
6. Q. T. Nguyen, M. Glasius, L. L. Sørensen, B. Jensen, H. Skov, W. Birmili, A. Wiedensohler, A. Kristensson, J. K. Nøjgaard, A. Massling, Seasonal variation of atmospheric particle number concentrations, new particle formation and atmospheric oxidation capacity at the high Arctic site Villum Research Station, Station Nord. *Atmos. Chem. Phys.* **16**, 11319–11336 (2016).
7. A. C. Lewis, J. R. Hopkins, L. J. Carpenter, J. Stanton, K. A. Read, M. J. Pilling, Sources and sinks of acetone, methanol, and acetaldehyde in North Atlantic marine air. *Atmos. Chem. Phys.* **5**, 1963–1974 (2005).
8. Y. Zhao, M. Saunois, P. Bousquet, X. Lin, A. Berchet, M. I. Hegglin, J. G. Canadell, R. B. Jackson, D. A. Hauglustaine, S. Szopa, A. R. Stavert, N. Luke Abraham, A. T. Archibald, S. Bekki, M. Deushi, P. Jöckel, B. Josse, D. Kinnison, O. Kirner, V. Marécal, F. M. O'Connor, D. A. Plummer, L. E. Revell, E. Rozanov, A. Stenke, S. Strode, S. Tilmes, E. J. Dlugokencky, B. Zheng, Inter-model comparison of global hydroxyl radical (OH) distributions and their impact on atmospheric methane over the 2000-2016 period. *Atmos. Chem. Phys.* **19**, 13701–13723 (2019).
9. B. Croft, R. V. Martin, W. Richard Leaitch, J. Burkart, R. Y. W. Chang, D. B. Collins, P. L. Hayes, A. L. Hodshire, L. Huang, J. K. Kodros, A. Moravek, E. L. Mungall, J. G. Murphy, S. Sharma, S. Tremblay, G. R. Wentworth, M. D Willis, J. P. D. Abbatt, J. R. Pierce, Arctic marine secondary organic aerosol contributes significantly to summertime particle size distributions in the Canadian Arctic Archipelago. *Atmos. Chem. Phys.* **19**, 2787–2812 (2019).
10. T. Cui, H. S. Green, P. W. Selleck, Z. Zhang, R. E. O'Brien, A. Gold, M. Keywood, J. H. Kroll, J. D. Surratt, Chemical Characterization of Isoprene- and Monoterpene-Derived Secondary Organic Aerosol Tracers in Remote Marine Aerosols over a Quarter Century. *ACS Earth Sp. Chem.* **3**, 935–946 (2019).
11. Q. H. Hu, Z. Q. Xie, X. M. Wang, H. Kang, Q. F. He, P. Zhang, Secondary organic aerosols over oceans via oxidation of isoprene and monoterpenes from Arctic to Antarctic. *Sci. Rep.* **3**, 1–7 (2013).
12. K. S. Carslaw, L. A. Lee, C. L. Reddington, K. J. Pringle, A. Rap, P. M. Forster, G. W. Mann, D. V. Spracklen, M. T. Woodhouse, L. A. Regayre, J. R. Pierce, Large contribution of natural aerosols to uncertainty in indirect forcing. *Nature* (2013), doi:10.1038/nature12674.
13. D. S. Hamilton, L. A. Lee, K. J. Pringle, C. L. Reddington, D. V. Spracklen, K. S. Carslaw, Occurrence of pristine aerosol environments on a polluted planet. *Proc. Natl. Acad. Sci. U. S. A.* **111**, 18466–18471 (2014).
14. K. J. Mayer, X. Wang, M. V. Santander, B. A. Mitts, J. S. Sauer, C. M. Sultana, C. D. Cappa, K. A. Prather, Secondary Marine Aerosol Plays a Dominant Role over Primary Sea Spray Aerosol in Cloud Formation. *ACS Cent. Sci.* **6**, 2259–2266 (2020).
15. D. V. Spracklen, S. R. Arnold, J. Sciare, K. S. Carslaw, C. Pio, Globally significant oceanic source of organic carbon aerosol. *Geophys. Res. Lett.* **35**, 1–5 (2008).
16. A. Hodzic, P. Campuzano-Jost, H. Bian, M. Chin, P. R. Colarco, D. A. Day, K. D. Froyd, B. Heinold, D. S. Jo, J. M. Katich, J. K. Kodros, B. A. Nault, J. R. Pierce, E. Ray, J. Schacht, G. P. Schill, J. C. Schroder, J. P. Schwarz, D. T. Sueper, I. Tegen, S. Tilmes, K. Tsigaridis, P. Yu, J. L. Jimenez, Characterization of organic aerosol across the global

remote troposphere: A comparison of ATom measurements and global chemistry models. *Atmos. Chem. Phys.* **20**, 4607–4635 (2020).
17. D. S. Alvim, J. B. Chiquetto, M. T. S. D'amelio, B. Khalid, D. L. Herdies, J. Pendharkar, S. M. Corrêa, S. N. Figueroa, A. Frassoni, V. B. Capistrano, C. Boian, P. Y. Kubota, P. Nobre, Evaluating carbon monoxide and aerosol optical depth simulations from cam-chem using satellite observations. *Remote Sens.* **13**, 1–36 (2021).
18. J. Schmale, A. Baccarini, I. Thurnherr, S. Henning, A. Efraim, L. Regayre, C. Bolas, M. Hartmann, A. Welti, K. Lehtipalo, F. Aemisegger, C. Tatzelt, S. Landwehr, R. L. Modini, F. Tummon, J. S. Johnson, N. Harris, M. Schnaiter, A. Toffoli, M. Derkani, N. Bukowiecki, F. Stratmann, J. Dommen, U. Baltensperger, H. Wernli, D. Rosenfeld, M. Gysel-Beer, Ken S. Carslaw, Overview of the Antarctic Circumnavigation Expedition: Study of Preindustrial-like Aerosols and Their Climate Effects (ACE-SPACE). *Bull. Am. Meterological Soc.* **101**, E1069–E1091 (2019).
19. A. Bodas-Salcedo, K. D. Williams, M. A. Ringer, I. Beau, J. N. S. Cole, J. L. Dufresne, T. Koshiro, B. Stevens, Z. Wang, T. Yokohata, Origins of the solar radiation biases over the Southern Ocean in CFMIP2 models. *J. Clim.* **27**, 41–56 (2014).
20. A. J. Schuddeboom, A. J. McDonald, The Southern Ocean Radiative Bias, Cloud Compensating Errors, and Equilibrium Climate Sensitivity in CMIP6 Models. *J. Geophys. Res. Atmos.* **126**, 1–16 (2021).
21. B. Rosati, S. Christiansen, R. Wollesen De Jonge, P. Roldin, M. M. Jensen, K. Wang, S. P. Moosakutty, D. Thomsen, C. Salomonsen, N. Hyttinen, J. Elm, A. Feilberg, M. Glasius, M. Bilde, New Particle Formation and Growth from Dimethyl Sulfide Oxidation by Hydroxyl Radicals. *ACS Earth Sp. Chem.* **5**, 801–811 (2021).
22. S. R. Arnold, D. V Spracklen, J. Williams, N. Yassaa, J. Sciare, B. Bonsang, V. Gros, I. Peeken, A. C. Lewis, I. Lsce, C. E. A. Saclay, S. Alvain, C. Moulin, Evaluation of the global oceanic isoprene source and its impacts on marine organic carbon aerosol. *Atmos. Chem. Phys.* **9**, 1253–1262 (2009).
23. A. Lee, A. H. Goldstein, J. H. Kroll, N. L. Ng, V. Varutbangkul, R. C. Flagan, J. H. Seinfeld, Gas-phase products and secondary aerosol yields from the photooxidation of 16 different terpenes. *J. Geophys. Res. Atmos.* **111**, 1–25 (2006).
24. N. L. Ng, J. H. Kroll, A. W. H. Chan, P. S. Chhabra, R. Flagan, J. H. Seinfeld, Secondary organic aerosol formation from m-xylene, toluene, and benzene. *Atmos. Chem. Phys.* **7**, 3909–3922 (2007).
25. D. Cabrera-Perez, D. Taraborrelli, R. Sander, A. Pozzer, Global atmospheric budget of simple monocyclic aromatic compounds. *Atmos. Chem. Phys.* **16**, 6931–6947 (2016).
26. J. B. Pernov, R. Bossi, T. Lebourgeois, J. K. Nøjgaard, R. Holzinger, L. Jens, H. Skov, Atmospheric VOC measurements at a High Arctic site : characteristics and source apportionment. *Atmos. Chem. Phys. Discuss.* (2020), doi:10.5194/acp-2020-528.
27. A. Colomb, V. Gros, S. Alvain, R. Sarda-Esteve, B. Bonsang, C. Moulin, T. Klupfel, J. Williams, Variation of atmospheric volatile organic compounds over the Southern Indian Ocean (30-49 degrees S). *Environ. Chem.* **6**, 70–82 (2009).
28. T. Guo, Z. Guo, J. Wang, J. Feng, H. Gao, X. Yao, Tracer-based investigation of organic aerosols in marine atmospheres from marginal seas of China to the northwest Pacific Ocean. *Atmos. Chem. Phys.* **20**, 5055–5070 (2020).
29. M. Rocco, E. Dunne, M. Peltola, N. Barr, J. Williams, A. Colomb, K. Safi, A. Saint-Macary, A. Marriner, S. Deppeler, J. Harnwell, C. Law, K. Sellegri, Oceanic phytoplankton are a potentially important source of benzenoids to the remote marine atmosphere. *Commun. Earth Environ.* **2**, 1–8 (2021).
30. P. K. Misztal, C. N. Hewitt, J. Wildt, J. D. Blande, A. S. D. Eller, S. Fares, D. R. Gentner, J. B. Gilman, M. Graus, J. Greenberg, A. B. Guenther, A. Hansel, P. Harley, M. Huang, K.

Jardine, T. Karl, L. Kaser, F. N. Keutsch, A. Kiendler-Scharr, E. Kleist, B. M. Lerner, T. Li, J. Mak, A. C. Nölscher, R. Schnitzhofer, V. Sinha, B. Thornton, C. Warneke, F. Wegener, C. Werner, J. Williams, D. R. Worton, N. Yassaa, A. H. Goldstein, Atmospheric benzenoid emissions from plants rival those from fossil fuels. *Sci. Rep.* **5**, 1–10 (2015).
31. C. A. Lawson, J. R. Seymour, M. Possell, D. J. Suggett, J. B. Raina, The Volatilomes of Symbiodiniaceae-Associated Bacteria Are Influenced by Chemicals Derived From Their Algal Partner. *Front. Mar. Sci.* **7**, 1–11 (2020).
32. M. C. Lemfack, B. O. Gohlke, S. M. T. Toguem, S. Preissner, B. Piechulla, R. Preissner, MVOC 2.0: A database of microbial volatiles. *Nucleic Acids Res.* **46**, D1261–D1265 (2018).
33. R. Romoli, M. C. Papaleo, D. De Pascale, M. L. Tutino, L. Michaud, A. Logiudice, R. Fani, G. Bartolucci, Characterization of the volatile profile of Antarctic bacteria by using solid-phase microextraction-gas chromatography-mass spectrometry. *J. Mass Spectrom.* **46**, 1051–1059 (2011).
34. R. Wanninkhof, OCEANOGRAPHY : METHODS Relationship between wind speed and gas exchange over the ocean revisited. *Limnol. Oceanogr. Methods*. **12**, 351–362 (2014).
35. S. J. Sjostedt, W. R. Leaitch, M. Levasseur, M. Scarratt, S. Michaud, J. Motard-Cté, J. H. Burkhart, J. P. D. Abbatt, Evidence for the uptake of atmospheric acetone and methanol by the Arctic Ocean during late summer DMS-Emission plumes. *J. Geophys. Res. Atmos.* **117**, 1–15 (2012).
36. É. A. Guérette, C. Paton-Walsh, I. Galbally, S. Molloy, S. Lawson, D. Kubistin, R. Buchholz, D. W. T. Griffith, R. L. Langenfelds, P. B. Krummel, Z. Loh, S. Chambers, A. Griffiths, M. Keywood, P. Selleck, D. Dominick, R. Humphries, S. R. Wilson, Composition of clean marine air and biogenic influences on VOCs during the MUMBA campaign. *Atmosphere (Basel).* **10**, 1–30 (2019).
37. T. C. Sauer, Volatile organic compounds in open ocean and coastal surface waters. *Org. Geochem.* **3**, 91–101 (1981).
38. C. A. Marandino, W. J. De Bruyn, S. D. Miller, E. S. Saltzman, Eddy correlation measurement of the air/sea flux of dimethylsulfide over the North Pacific Ocean. *J. Geophys. Res. Atmos.* **112**, 1–12 (2007).
39. J. F. Lamarque, L. K. Emmons, P. G. Hess, D. E. Kinnison, S. Tilmes, F. Vitt, C. L. Heald, E. A. Holland, P. H. Lauritzen, J. Neu, J. J. Orlando, P. J. Rasch, G. K. Tyndall, CAM-chem: Description and evaluation of interactive atmospheric chemistry in the Community Earth System Model. *Geosci. Model Dev.* **5**, 369–411 (2012).
40. P. Prakash, S. Prakash, M. Ravichandran, T. V. S. U. Bhaskar, N. A. Kumar, Seasonal evolution of chlorophyll in the Indian sector of the Southern Ocean: Analyses of Bio-Argo measurements. *Deep. Res. Part II Top. Stud. Oceanogr.* **178**, 104791 (2020).
41. S. G. Wakeham, E. A. Canuel, P. H. Doering, Geochemistry of volatile organic compounds in seawater: Mesocosm experiments with 14C-model compounds. *Geochim. Cosmochim. Acta*. **50**, 1163–1172 (1986).
42. J. Wang, K. Sandoval, Y. Ding, D. Stoeckel, A. Minard-Smith, G. Andersen, E. A. Dubinsky, R. Atlas, P. Gardinali, Biodegradation of dispersed Macondo crude oil by indigenous Gulf of Mexico microbial communities. *Sci. Total Environ.* **557**–**558**, 453–468 (2016).
43. P. K. Misztal, C. N. Hewitt, J. Wildt, J. D. Blande, A. S. D. Eller, S. Fares, D. R. Gentner, J. B. Gilman, M. Graus, J. Greenberg, A. B. Guenther, A. Hansel, P. Harley, M. Huang, K. Jardine, T. Karl, L. Kaser, F. N. Keutsch, A. Kiendler-Scharr, E. Kleist, B. M. Lerner, T. Li, J. Mak, A. C. Nölscher, R. Schnitzhofer, V. Sinha, B. Thornton, C. Warneke, F. Wegener, C. Werner, J. Williams, D. R. Worton, N. Yassaa, A. H. Goldstein, Atmospheric benzenoid emissions from plants rival those from fossil fuels. *Sci. Rep.* **5** (2015),

doi:10.1038/srep12064.
44. P. Rodríguez-Ros, P. Cortés, C. M. Robinson, S. Nunes, C. Hassler, S. J. Royer, M. Estrada, M. M. Sala, R. Simó, Distribution and drivers of marine isoprene concentration across the Southern Ocean. *Atmosphere (Basel).* **11**, 1–19 (2020).
45. C. Wohl, I. Brown, V. Kitidis, A. E. Jones, W. T. Sturges, P. Nightingale, M. Yang, D. Philip, P. Nightingale, M. Yang, D. Philip, Underway seawater and atmospheric measurements of volatile organic compounds in the Southern Ocean. *Biogeosciences*. **17**, 2593–2619 (2020).
46. M. J. Kim, G. A. Novak, M. C. Zoerb, M. Yang, B. W. Blomquist, B. J. Huebert, C. D. Cappa, T. H. Bertram, Air-Sea exchange of biogenic volatile organic compounds and the impact on aerosol particle size distributions. *Geophys. Res. Lett.* **44**, 3887–3896 (2017).
47. S. J. Lawson, C. S. Law, M. J. Harvey, T. G. Bell, C. F. Walker, W. J. De Bruyn, E. S. Saltzman, Methanethiol, dimethyl sulfide and acetone over biologically productive waters in the southwest Pacific Ocean. *Atmos. Chem. Phys.* **20**, 3061–3078 (2020).
48. A. Randelhoff, L. Oziel, P. Massicotte, G. Bécu, M. Galí, L. Lacour, D. Dumont, A. Vladoiu, C. Marec, F. Bruyant, M. N. Houssais, J. É. Tremblay, G. Deslongchamps, M. Babin, The evolution of light and vertical mixing across a phytoplankton ice-edge bloom. *Elementa*. **7** (2019), doi:10.1525/elementa.357.
49. M. Galí, M. Lizotte, D. J. Kieber, A. Randelhoff, R. Hussherr, L. Xue, J. Dinasquet, M. Babin, E. Rehm, M. Levasseur, DMS emissions from the Arctic marginal ice zone. *Elementa*. **9** (2021), doi:10.1525/elementa.2020.00113.
50. C. Wohl, A. Jones, W. Sturges, P. Nightingale, B. Else, B. Butterworth, M. Yang, Sea ice concentration impacts dissolved organic gases in the Canadian Arctic. *Biogeosciences*. **19**, 1021–1045 (2022).
51. T. M. Burgers, J.-É. Tremblay, B. G. T. Else, T. N. Papakyriakou, Estimates of net community production from multiple approaches surrounding the spring ice-edge bloom in Baffin Bay. *Elem. Sci. Anthr.* **8** (2020), doi:10.1525/elementa.013.
52. J. Pernov, R. Bossi, T. Lebourgeois, J. Nøjgaard, R. Holzinger, J. Hjorth, H. Skov, Atmospheric VOC measurements at a High Arctic site: characteristics and source apportionment. *Atmos. Chem. Phys.* **21**, 2895–2916 (2020).
53. P. Rodríguez-Ros, M. Galí, P. Cortés, C. M. Robinson, D. Antoine, C. Wohl, M. X. Yang, R. Simó, Remote Sensing Retrieval of Isoprene Concentrations in the Southern Ocean. *Geophys. Res. Lett.* **47** (2020), doi:10.1029/2020GL087888.
54. D. Taraborrelli, D. Cabrera-Perez, S. Bacer, S. Gromov, J. Lelieveld, R. Sander, A. Pozzer, Influence of aromatics on tropospheric gas-phase composition. *Atmos. Chem. Phys.* **21**, 2615–2636 (2021).
55. D. Lubin, D. Zhang, I. Silber, R. C. Scott, P. Kalogeras, A. Battaglia, D. H. Bromwich, M. Cadeddu, E. Eloranta, A. Fridlind, A. Frossard, K. M. Hines, S. Kneifel, W. R. Leaitch, W. Lin, J. Nicolas, H. Powers, P. K. Quinn, P. Rowe, L. M. Russell, S. Sharma, J. Verlinde, A. M. Vogelmann, AWARE: The atmospheric radiation measurement (ARM) west antarctic radiation experiment. *Bull. Am. Meteorol. Soc.* **101**, E1069–E1091 (2020).
56. X. Cheng, Q. Chen, Y. J. Li, Y. Zheng, K. Liao, G. Huang, Highly Oxygenated Organic Molecules Produced by the Oxidation of Benzene and Toluene in a Wide Range of OH Exposure and NO_x Conditions. *Atmos. Chem. Phys.*, 1–23 (2021).
57. V. Pospisilova, F. D. Lopez-Hilfiker, D. M. Bell, I. El Haddad, C. Mohr, W. Huang, L. Heikkinen, M. Xiao, J. Dommen, A. S. H. Prevot, U. Baltensperger, J. G. Slowik, On the fate of oxygenated organic molecules in atmospheric aerosol particles. *Sci. Adv.* **6**, 1–12 (2020).
58. C. Tatzelt, S. Henning, A. Welti, A. Baccarini, M. Hartmann, M. Gysel-Beer, M. Van Pinxteren, R. L. Modini, J. Schmale, F. Stratmann, S. H. De), Circum-Antarctic abundance

and properties of CCN and INP. *Atmos. Chem. Phys. Discuss.* **In review**, 1–35 (2021).
59. C. Wohl, D. Capelle, A. Jones, W. T. Sturges, P. D. P. D. P. D. Nightingale, B. G. T. T. Else, M. Yang, Segmented flow coil equilibrator coupled to a Proton Transfer Reaction Mass Spectrometer for measurements of a broad range of Volatile Organic Compounds in seawater. *Ocean Sci.* **15**, 1–37 (2019).
60. C. Warneke, J. A. De Gouw, W. C. Kuster, P. D. Goldan, R. Fall, Validation of atmospheric VOC measurements by proton-transfer-reaction mass spectrometry using a gas-chromatographic preseparation method. *Environ. Sci. Technol.* **37**, 2494–2501 (2003).
61. P. S. Liss, P. G. Slater, Flux of Gases across the Air-Sea Interface. *Nature*. **247**, 181–184 (1974).
62. P. D. Nightingale, G. Malin, C. S. Law, J. Watson, P. S. Liss, I. Liddicoat, In situ evaluation of air-sea gas exchange parameterizations using novel conservative and volatile tracers. *Global Biogeochem. Cycles*. **14**, 373–387 (2000).
63. M. Yang, P. D. Nightingale, R. Beale, P. S. Liss, B. W. Blomquist, C. W. Fairall, Atmospheric deposition of methanol over the Atlantic Ocean. *Proc. Natl. Acad. Sci. U. S. A.* **110**, 20034–9 (2013).
64. M. T. Johnson, A numerical scheme to calculate temperature and salinity dependent air-water transfer velocities for any gas. *Ocean Sci.* **6**, 913–932 (2010).
65. J. Prytherch, I. M. Brooks, P. M. Crill, B. F. Thornton, D. J. Salisbury, M. Tjernström, L. G. Anderson, M. C. Geibel, C. Humborg, Direct determination of the air-sea CO2 gas transfer velocity in Arctic sea ice regions. *Geophys. Res. Lett.* **44**, 3770–3778 (2017).
66. A. Saiz-Lopez, J. F. Lamarque, D. E. Kinnison, S. Tilmes, C. Ordóñez, J. J. Orlando, A. J. Conley, J. M. C. Plane, A. S. Mahajan, G. Sousa Santos, E. L. Atlas, D. R. Blake, S. P. Sander, S. Schauffler, A. M. Thompson, G. Brasseur, Estimating the climate significance of halogen-driven ozone loss in the tropical marine troposphere. *Atmos. Chem. Phys.* **12**, 3939–3949 (2012).
67. D. A. Lack, X. X. Tie, N. D. Bofinger, A. N. Wiegand, S. Madronich, Seasonal variability of secondary organic aerosol: A global modeling study. *J. Geophys. Res. Atmos.* **109** (2004), doi:10.1029/2003jd003418.
68. J. R. Odum, T. Hoffmann, F. Bowman, D. Collins, R. C. Flagan, J. H. Seinfeld, Gas/particle partitioning and secondary organic aerosol yields. *Environ. Sci. Technol.* **30**, 2580–2585 (1996).
69. B. N. Murphy, S. N. Pandis, Simulating the formation of semivolatile primary and secondary organic aerosol in a regional chemical transport model. *Environ. Sci. Technol.* **43**, 4722–4728 (2009).
70. A. Mahmud, K. Barsanti, Improving the representation of secondary organic aerosol (SOA) in the MOZART-4 global chemical transport model. *Geosci. Model Dev.* **6**, 961–980 (2013).
71. M. S. Choi, X. Qiu, J. Zhang, S. Wang, X. Li, Y. Sun, J. Chen, Q. Ying, Study of Secondary Organic Aerosol Formation from Chlorine Radical-Initiated Oxidation of Volatile Organic Compounds in a Polluted Atmosphere Using a 3D Chemical Transport Model. *Environ. Sci. Technol.* **54**, 13409–13418 (2020).
72. Q. Li, X. Fu, X. Peng, W. Wang, A. Badia, R. P. Fernandez, C. A. Cuevas, Y. Mu, J. Chen, J. L. Jimenez, T. Wang, A. Saiz-Lopez, Halogens Enhance Haze Pollution in China. *Environ. Sci. Technol.* **55**, 13625–13637 (2021).
73. M. J. Gidden, K. Riahi, S. J. Smith, S. Fujimori, G. Luderer, E. Kriegler, D. P. Van Vuuren, M. Van Den Berg, L. Feng, D. Klein, K. Calvin, J. C. Doelman, S. Frank, O. Fricko, M. Harmsen, T. Hasegawa, P. Havlik, J. Hilaire, R. Hoesly, J. Horing, A. Popp, E. Stehfest, K. Takahashi, Global emissions pathways under different socioeconomic scenarios for use in CMIP6: A dataset of harmonized emissions trajectories through the end

of the century. *Geosci. Model Dev.* **12**, 1443–1475 (2019).
74. A. Guenther, T. Karl, P. Harley, C. Weidinmyer, P. I. Palmer, C. Geron, Edinburgh Research Explorer Estimates of global terrestrial isoprene emissions using MEGAN (Model of Emissions of Gases and Aerosols from Nature) and Physics Estimates of global terrestrial isoprene emissions using MEGAN (Model of Emissions of Gases an. *Atmos. Chem. Phys.*, 3181–3210 (2006).
75. S. Tilmes, J. F. Lamarque, L. K. Emmons, D. E. Kinnison, D. Marsh, R. R. Garcia, A. K. Smith, R. R. Neely, A. Conley, F. Vitt, M. Val Martin, H. Tanimoto, I. Simpson, D. R. Blake, N. Blake, Representation of the Community Earth System Model (CESM1) CAM4-chem within the Chemistry-Climate Model Initiative (CCMI). *Geosci. Model Dev.* **9**, 1853–1890 (2016).
76. P. R. Veres, J. Andrew Neuman, T. H. Bertram, E. Assaf, G. M. Wolfe, C. J. Williamson, B. Weinzierl, S. Tilmes, C. R. Thompson, A. B. Thames, J. C. Schroder, A. Saiz-Lopez, A. W. Rollins, J. M. Roberts, D. Price, J. Peischl, B. A. Nault, K. H. Møller, D. O. Miller, S. Meinardi, Q. Li, J. F. Lamarque, A. Kupc, H. G. Kjaergaard, D. Kinnison, J. L. Jimenez, C. M. Jernigan, R. S. Hornbrook, A. Hills, M. Dollner, D. A. Day, C. A. Cuevas, P. Campuzano-Jost, J. Burkholder, T. Paul Bui, W. H. Brune, S. S. Brown, C. A. Brock, I. Bourgeois, D. R. Blake, E. C. Apel, T. B. Ryerson, Global airborne sampling reveals a previously unobserved dimethyl sulfide oxidation mechanism in the marine atmosphere. *Proc. Natl. Acad. Sci. U. S. A.* **117**, 4505–4510 (2020).
77. Amundsen Science Data Collection, TSG and CTD data collected by the CCGS Amundsen in the Canadian Arctic. Processed data. TSG Version 2. CTD Version 1. Archived at www.polardata.ca, Canadian Cryospheric Information Network (CCIN). *ArcticNet Inc., Québec, Canada.* (2017), doi:TSG: https://doi.org/10.5884/12715. Accessed on 14/09/21.CTD: https://www.polardata.ca/pdcsearch/?doi_id=12713 Accessed on 14/09/21.

Acknowledgments

Funding

European Union Horizon 2020 grant SUMMIT ERC-2018-AdG 834162 (RS)
Spanish National Research Council grant PEGASO CTM2012-37615 (RS)
'Severo Ochoa Centre of Excellence' accreditation grant CEX2019-000928-S
European Union Horizon 2020 grant CLIMAHAL ERC-2016- COG 726349 (ASL)
UK Research and Innovation grant ORCHESTRA NE/N018095/1
National Science Foundation grant CESM
Computing resources, support, and data storage were provided by the Climate Simulation Laboratory at NCAR's Computational and Information Systems Laboratory (CISL), sponsored by the NSF.

Author contributions:

Conceptualization: CW, MY, RS
Methodology: CW, MY, QL, CAC, RPF, ASL
CAM-Chem model development and simulations: QL, CAC, RPF, ASL
Investigation: CW
Supervision: RS, MY
Writing—original draft: CW
Writing—review & editing: CW, RS, MY, QL, CAC, RPF, ASL
Funding acquisition: RS, ASL, MY

Competing interests: Authors declare that they have no competing interests.

Data and materials availability: All data needed to evaluate the conclusions of the paper are present in the paper and/or the Supplementary Materials. The measurements and fluxes from the Southern Ocean can be accessed through the following DOI: https://doi.org/10.5281/zenodo.6523780 (last access 06.05.2022). The measurements and fluxes from the Arctic can be accessed through this DOI: https://doi.org/10.21963/13271. The CAM-Chem (the public version) code is available on: https://www2.acom.ucar.edu/gcm/cam-chem (last access 28.04.2022).

Figures and Tables

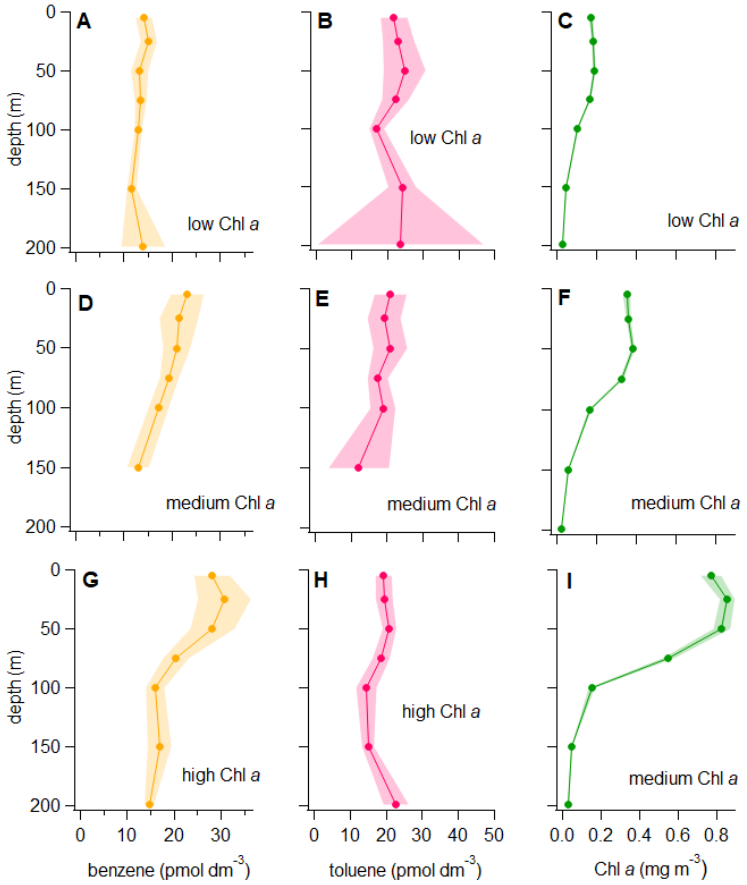

Figure 1 Overview plot displaying depth bin averaged casts of benzene (A, D G), toluene (B, E, H) and Chl *a* (G, F, I) from the Southern Ocean cruise. The casts are grouped by surface Chl *a* concentration (low, medium and high Chl *a*) and depth bin averaged. The grey shaded area indicates the standard error of each depth bin. Depth bins containing less than 2 data points are not shown to avoid bias. The number of individual casts in each Chl *a* group is 11 for low Chl *a*, 10 for medium Chl *a* and 7 for high Chl *a*.

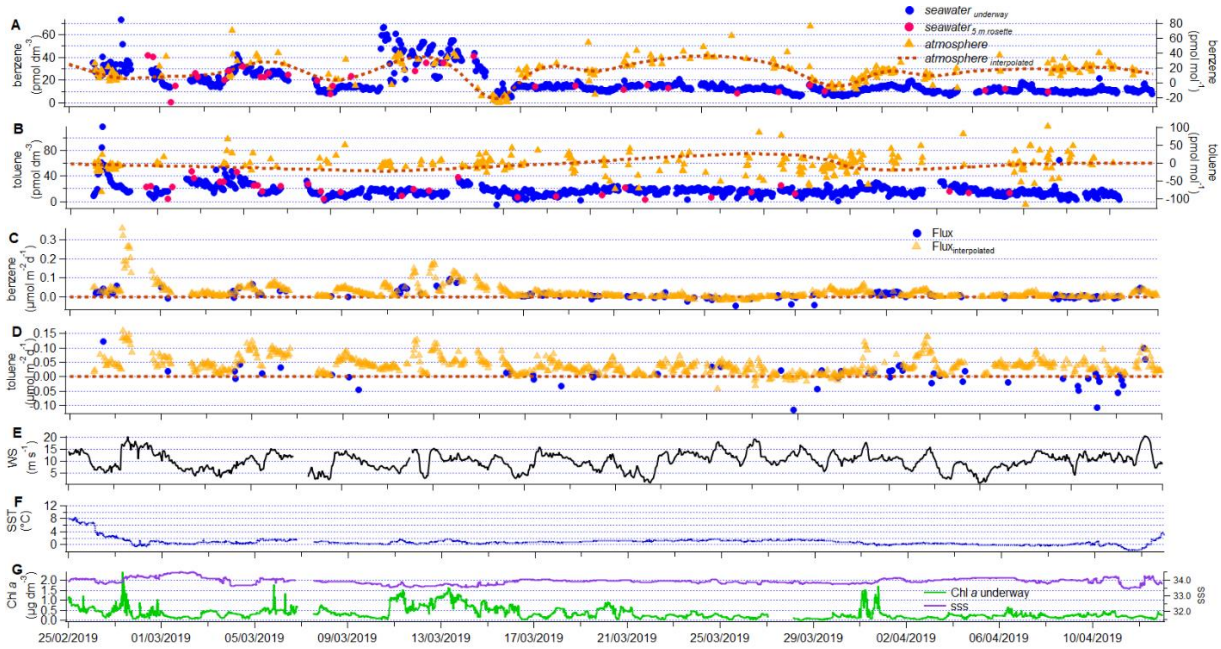

Figure 2 Benzene and toluene underway surface seawater concentrations, atmospheric mole fractions ((A) and (B)), and air–sea fluxes ((C) and (D)) from the Southern Ocean cruise. Positive fluxes indicate ocean outgassing i.e. sea-to-air fluxes. Other panels show the wind speed (WS) (E), underway sea surface temperature (SST) (F) as well as Chl *a* and surface seawater salinity (SSS) (G).

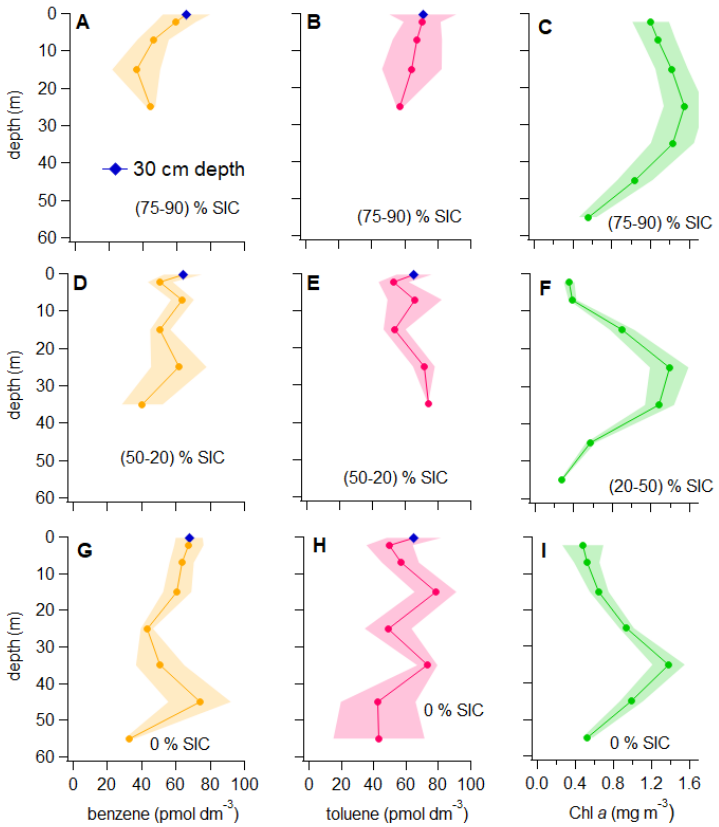

Figure 3 Depth bin averaged casts of benzene (A, D,G), toluene (B, E, H) and Chl *a* (C, F, I), grouped by sea ice cover (SIC), from the Arctic cruise. The casts are grouped by sea ice cover and depth bin averaged. The grey shaded area indicates the standard error of each depth bin. Depth bins containing less than 2 data points are not shown to avoid bias. The number of individual casts in each SIC group is 4 for 75–90 %, 7 for 20–50 % and 13 for 0 % SIC.

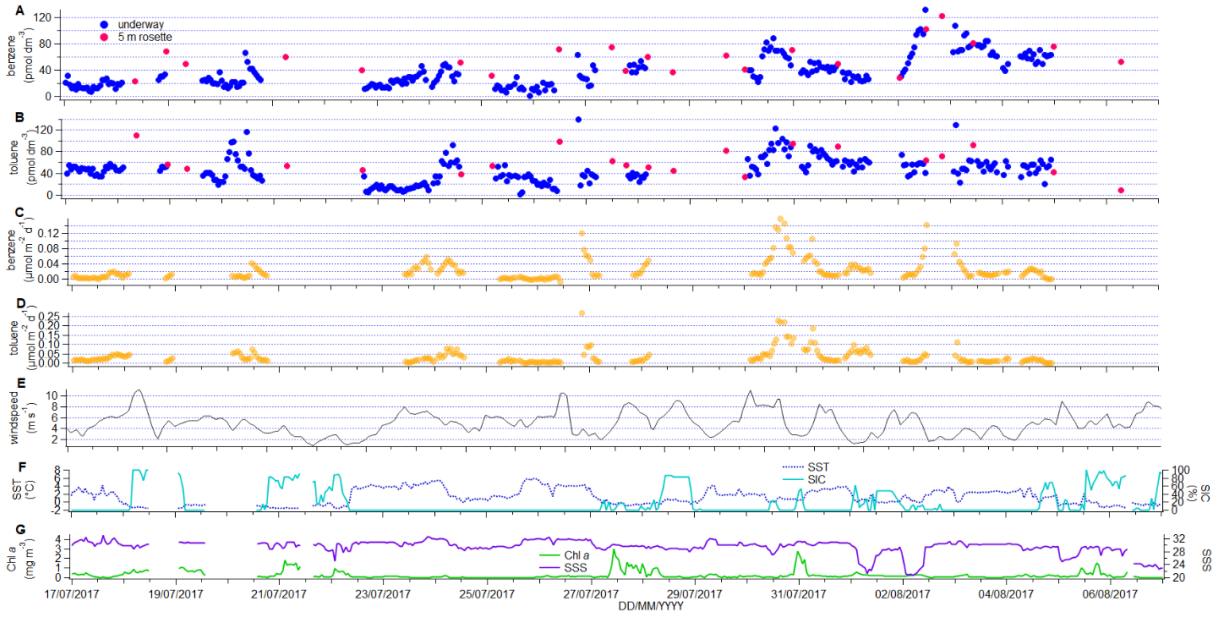

Figure 4 Benzene and toluene underway surface seawater concentrations ((A) and (B)) and air–sea fluxes ((C) and (D)) from the Arctic marginal sea ice zone. Positive fluxes indicate ocean outgassing i.e. sea-to-air flux. Other panels show the wind speed (E), underway sea surface temperature (SST) and sea ice cover (SIC, AMSR2) (F) as well as Chl *a* and surface seawater salinity (SSS) (G).

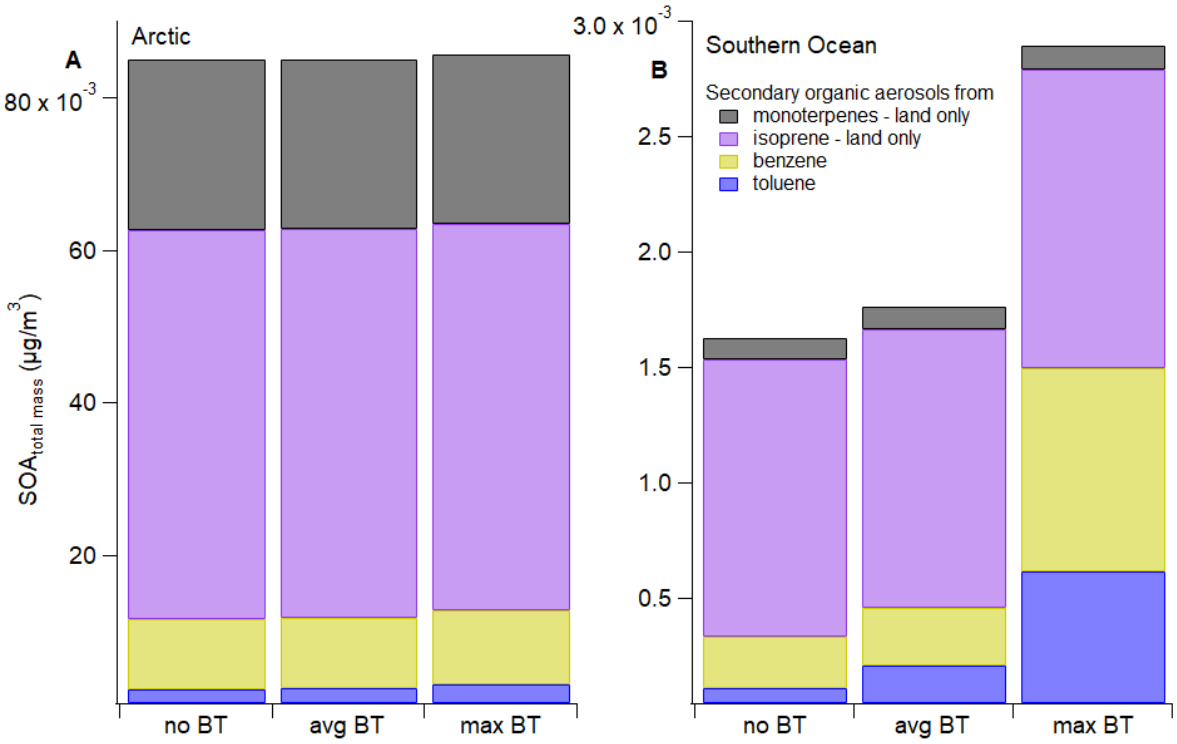

Figure 5 Impact of benzene and toluene ocean emission fluxes on secondary organic aerosol mass concentrations in (A) the Arctic (Jul–Aug 2017) and (B) the Southern Ocean (Feb–Apr 2019). Three model runs are presented that differ by their ocean benzene and toluene ocean emissions; "no BT" = no ocean benzene/toluene fluxes, "avg BT" = mean benzene/toluene ocean fluxes, "max BT" = highest measured benzene/toluene fluxes.

Table 1 Modelling results showing the impact of benzene and toluene emissions on atmospheric benzene, toluene and OH mole fractions in the polar regions. Sampling months were Feb–Mar 2019 for the Southern Ocean and Jul–Aug 2017 for the Arctic. Three model runs were; "no BT" = no ocean benzene/toluene fluxes, "avg BT" = mean benzene/toluene ocean fluxes, "max BT" = highest measured benzene/toluene fluxes (See Supplement S2). "absdiff" = absolute difference, "reldiff" = relative difference or relative change**.**

		no BT	avg BT			max BT		
		Mole fractions (pmol mol^{-1})	Mole fractions (pmol mol^{-1})	Absdiff (pmol mol^{-1})	Reldiff (%)	Mole fractions (pmol mol^{-1})	Absdiff (pmol mol^{-1})	Reldiff (%)
Arctic	Benzene	19.7	22.1	2.4	12	34.8	15.1	77
	Toluene	1.7	3.4	1.7	100	15.7	14.0	824
	OH	0.06	0.06	0	<0.01	0.06	0	<0.02
Antarctic	Benzene	0.9	4.1	3.2	355	48.3	47.4	5059
	Toluene	0.1	3.1	3.0	3000	12.1	12.0	12000
	OH	0.008	0.008	0	<0.01	0.008	0	<0.01

762

763

764

Supplementary Materials

Supplementary Text

Details on the Chl a data from both cruises.

Chl *a* data from both cruises in depth profiles and underway are from fluorescence sensors. The underway Chl *a* data from the Antarctic cruise are relatively uncertain due to large sensor drift, but the data has been corrected using the sensor mounted on the CTD frame. For the Arctic cruise, Chl *a* measured from CTD frame and underway agree within 0.1 mg m^{-3}. Thus, our Chl *a* data does not explicitly account for quenching of fluorescence and is not proportional to phytoplankton biomass. It is of value to compare Chl *a* with benzene and toluene distributions in depth profiles and underway data to obtain information on the possible biological source, though it is not possible to derive from this how benzene and toluene concentrations correlate with phytoplankton biomass.

Details on the computation of benzene and toluene seawater and ambient air concentrations as well as fluxes

During the Antarctic cruise, the PTR-MS was calibrated weekly using a certified gas standard (Apel–Riemer Inc.). During the Arctic cruise, benzene was calibrated using a certified gas standard during installation before the campaign. A post-cruise calibration with a certified gas standard was applied to toluene. These calibration curves were used to calculate equilibrator headspace gas phase mole fractions and ambient air mole fractions. During the Arctic cruise, this gas calibration displayed a humidity dependence for benzene and toluene, which was not observed during the Antarctic deployment due to the higher drift tube voltage.

To calculate ambient air measurements, hourly measurement of outside air scrubbed by a 450°C Pt-catalyst is used as a blank for toluene. Daily measurements of zero air carrier gas are used as a blank for benzene. Measurement of zero air from a gas canister are used as a blank for benzene because it seemed that during episodes of high benzene air mole fractions from sampling ship exhaust the Pt-catalyst does not fully remove benzene. For most of the deployment, the Pt-catalyst agrees with the zero air.

For both cruises, benzene and toluene seawater concentrations were calculated using the equations and solubilities laid out in Wohl et al. (*59*). As laid out elsewhere (Supplement of Wohl et al. (*45*) and Wohl et al. (*50*)), the choice of measurement background is critical. Here we lay out what blanks are used to compute seawater concentrations for both deployments. Please see the supplements of Wohl et al. (*45*) and Wohl et al. (*50*) for detailed definitions of the blanks cited here. For the Antarctic deployment, zero air measurement was used as a blank for benzene seawater measurement. Due to the humidity dependence of the toluene background, we used humid air (air of the same humidity as equilibrator headspace scrubbed by a Pt-catalyst) as a blank for the seawater measurement. Similarly, the Arctic measurements are presented with zero air as a blank for benzene and the wet equilibrator air (zero air which has passed through the empty wet equilibrator) as a blank for toluene. Small differences in the cruise mean concentration presented here and in Wohl et al. (*59*) are due to different choices of background. Concentrations shown here should be cited in the future as they incorporate an improved understanding of the SFCE-PTR-MS system. We thus use zero air as a background for benzene and a measurement of air of similar humidity as equilibrator headspace as a background for toluene on both cruises.
For both cruises, CTD measurements at 5m and underway measurements agree very well suggesting no contamination from either sampling technique. In Wohl et al. (*59*), we discuss that average concentrations of toluene measured from

the underway inlet are slightly higher than those measured from the underway inlet. In this manuscript, we display measurements from both sampling techniques which show no obvious bias. It is possible that mean underway concentrations are slightly higher as they by chance capture episodes of higher concentrations during this cruise. We note that for the Antarctic cruise, benzene and toluene seawater measurements did not appear to be affected by photochemical production within the SFCE.

The measurement noise (Table S1) is calculated as the standard deviation of the residual of the interpolation of the measurement background (as laid out in Wohl et al. (*45*)). The limit of detection is defined as three times the measurement noise. Measurement noise was calculated to be 8 and 10 pmol mol^{-1} for benzene and toluene in the air. The measurement noise in seawater for the Southern Ocean cruise was 1 and 4 pmol dm^{-3} for benzene and toluene while it was 5 and 10 pmol dm^{-3} for benzene and toluene during the Arctic cruise.

The seawater measurement noise is slightly higher in the Arctic compared to the Southern Ocean cruise due to less frequent blanks and different PTR-MS quadrupole data collection settings. Measurement noise and LOD are low enough to detect these gases in seawater while air mole fractions were often close to the LOD.

Fig. S1.

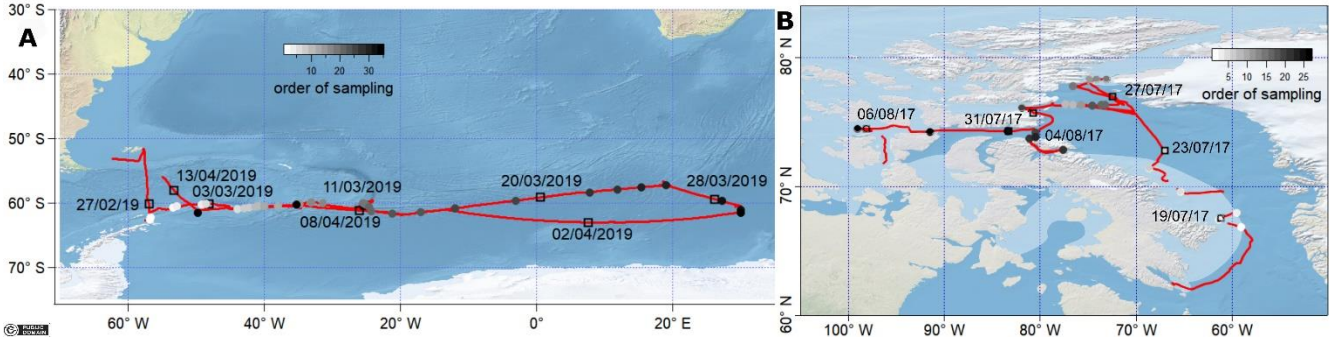

Figure S1 Map illustrating the cruise sampling tracks in red in the Southern Ocean (A) and the Arctic (B). Location of the CTD stations is indicated by a filled circle coloured by the order of sampling. Hollow squares and date labels (DD/MM/YYY) are used to give an indication of the sampling date. Interruptions in the cruise track and underway auxiliary data (B) are due to interruptions in the ship underway logging system (*77*). All the map data were created from public domain GIS data found on the Natural Earth website (http://www.naturalearthdata.com, last access: 15 April 2021). They were read into Igor using the Igor GIS XOP beta. The sea-ice-covered area during the Arctic cruise (B) is approximately indicated for illustration purposes as a shaded area due to the dynamic nature of sea ice and difficulties in conveying this information for a month-long deployment. The approximate location of the sea ice edge is based on the average sea ice cover for the whole cruise duration using AMSR2 satellite data.

The cruise sampling tracks of the two cruises in the polar oceans are presented in Figure S1. One of the cruises focussed on sampling the remote Southern Ocean during austral summer and autumn from 21 February to 15 April 2019 on board the RRS *James Clark Ross*. The vessel transited south from the Falkland Islands to the Antarctic Peninsula. For most of the cruise, it then followed approximately 60° S in latitude eastwards, while sampling a large number of CTD (Conductivity/Temperature/Depth) stations, until reaching 30° E. Then the vessel made the return journey and completed a few more CTD stations on its transit back. Essentially no sea ice was encountered during this cruise, only icebergs. The second cruise focused on sampling the marginal sea ice zone in the Canadian Arctic during boreal summer from 17 July until 8 August 2017 on board the icebreaker CCGS *Amundsen*. The research vessel travelled northwards through Davis Straight to Baffin Bay to reach Smith Sound, where more intense depth profile sampling was undertaken. From there the vessel transited east into the Canadian Arctic Archipelago. Further details of the cruise sampling track and strategy are presented in Wohl et al. (*45*, *50*).

Fig. S2.

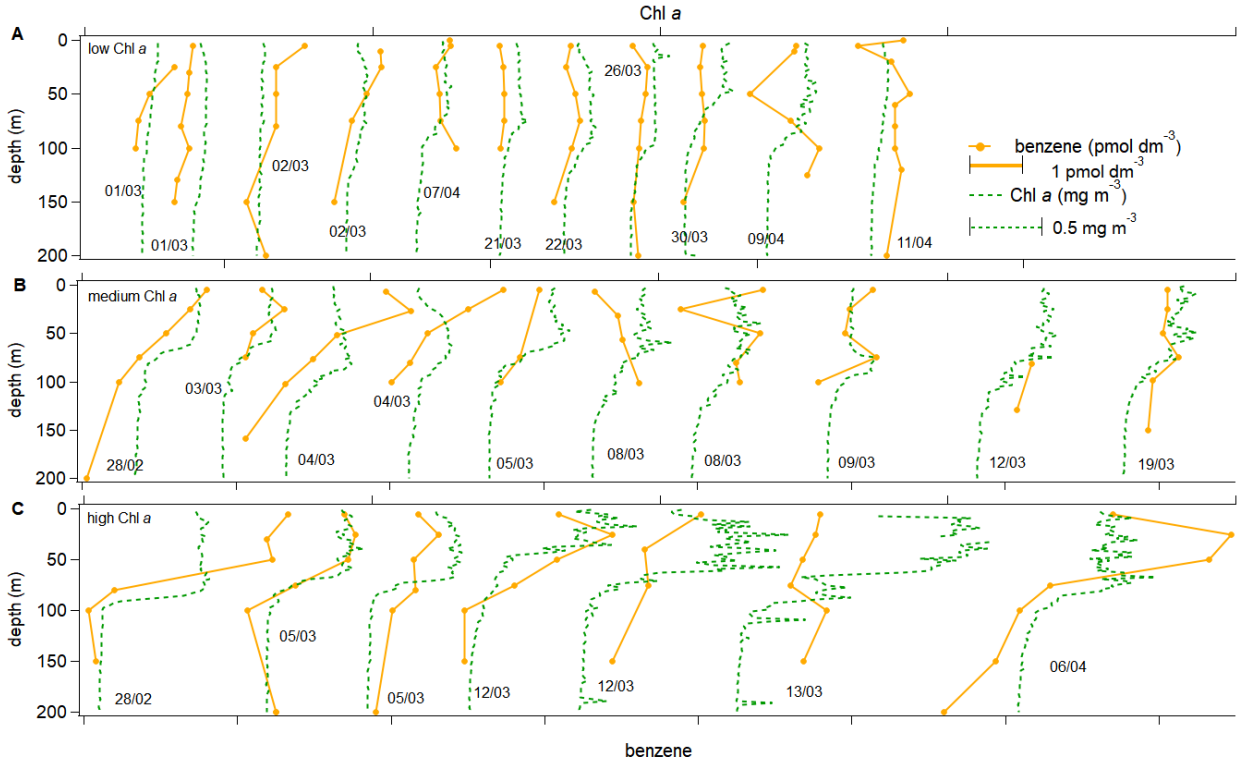

Figure S2 Overview plot displaying the shape of all benzene and Chl *a* depth profiles from the Southern Ocean. The casts are grouped in panels by surface Chl *a* concentration (low, medium and high Chl *a*) and staggered along the x-axis for ease of viewing. The scale bars for benzene and Chl *a* in panel (A) also apply to panels (B) and (C). Date labels indicate sampling dates (DD/MM).

Fig. S3.

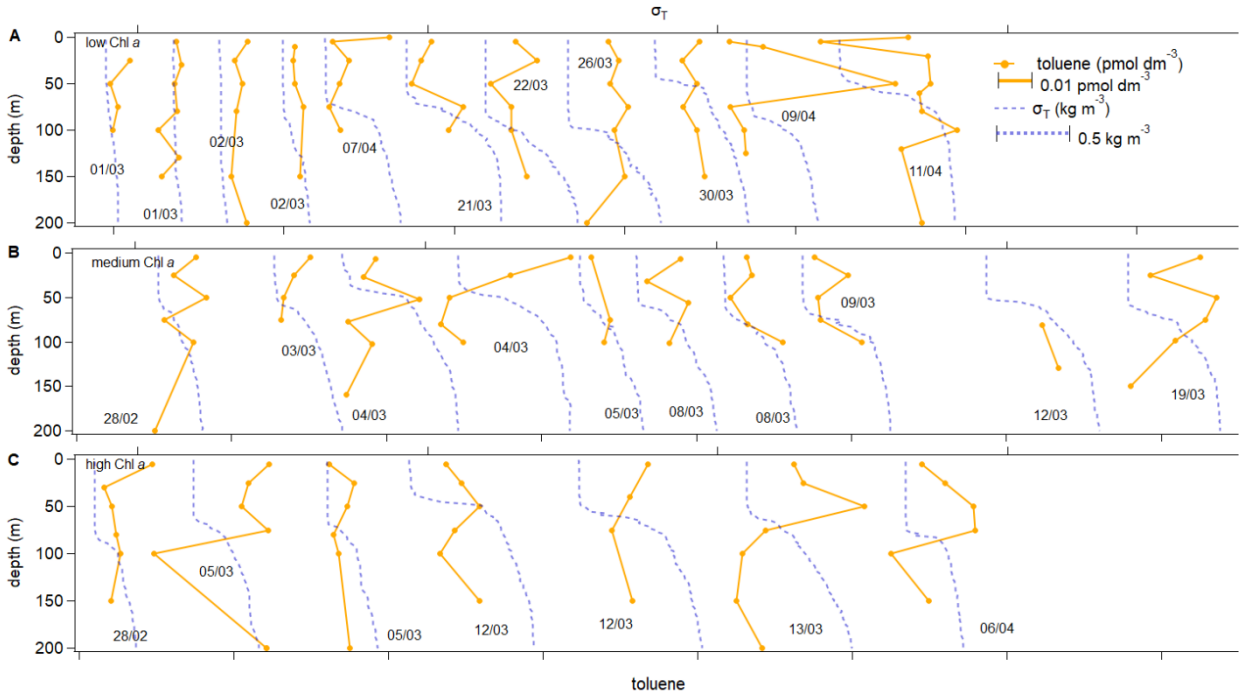

Figure S3 Overview plot displaying the shape of all toluene and density depth profiles from the Southern Ocean. The casts are grouped in panels by surface Chl a concentration (low, medium and high Chl a) and staggered along the x-axis for ease of viewing. The scale bars for toluene and Chl a in panel (A) also apply to panels (B) and (C). Date labels indicate sampling dates (DD/MM).

Fig. S4.

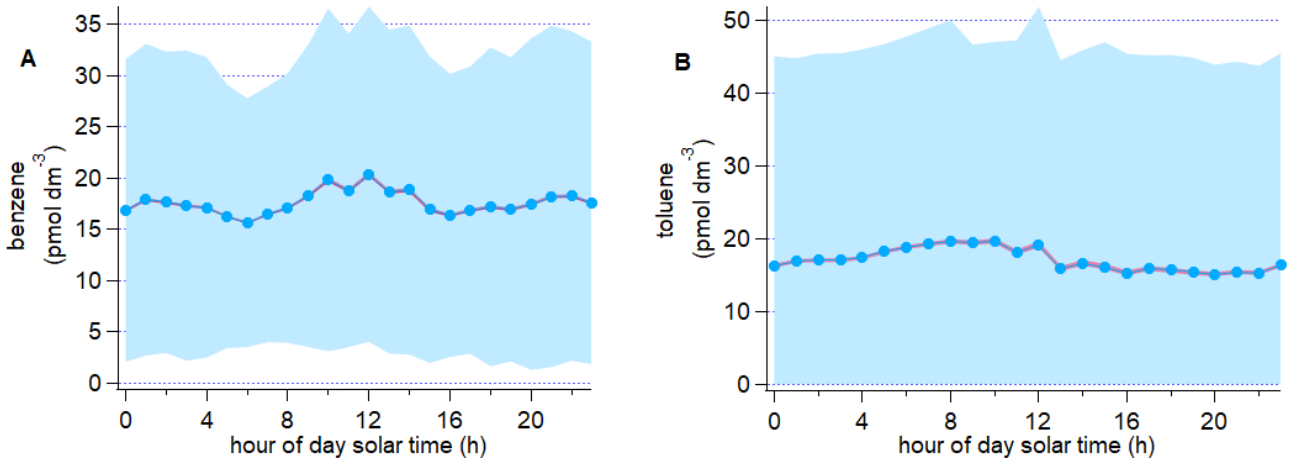

Figure S4 Diurnal changes in seawater concentrations of (A) benzene and (B) toluene in underway surface seawater. Light blue shaded area indicates the standard deviation of each hourly bin and the pink shaded area indicates the standard error of each bin.

We test for diurnal variability in the measured seawater concentrations from the Southern Ocean by using the local solar time to remove the influence of the ship track crossing multiple time zones. The measured seawater concentrations were binned in 24 hourly bins and the standard deviation and standard error was calculated for each bin (Figure S2). Figure S2 shows that measurements of benzene and toluene during solar zenith are generally a little higher than the other measurements, but there is no substantial diurnal variability in seawater benzene and toluene concentrations and this variability is not statistically significant. The Arctic data was not tested for diurnal variability due to 24 h light during the sampling period and the relatively smaller dumber of data points compared to the Southern Ocean cruise.

884 **Fig. S5.**

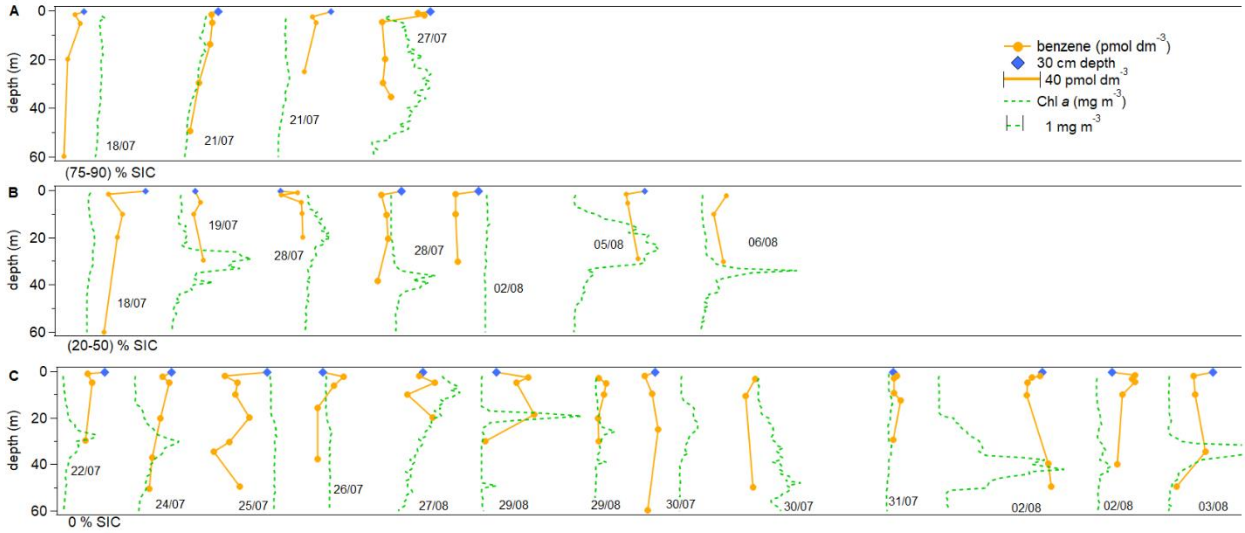

885
886 **Figure S5 Overview plot displaying the shape of all benzene and Chl *a* depth profiles, grouped by SIC.** Panel labels
887 indicate the SIC bin. The scale bars for benzene and Chl *a* in panel (A) apply also to panels (B) and (C). One of the Chl *a* profiles
888 is cut off in panel (C) for scale purposes.
889
890
891
892
893

894 **Fig. S6.**

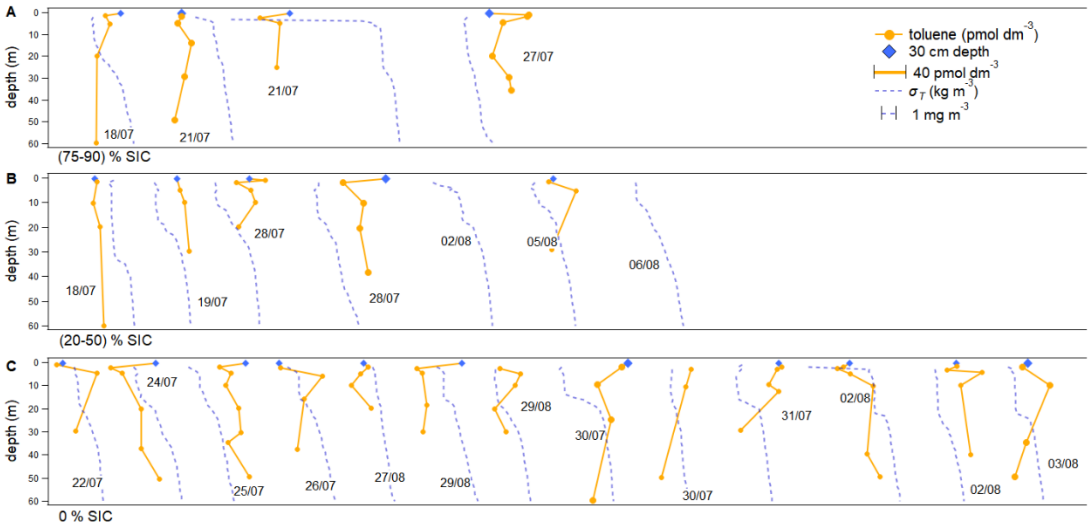

895
896 **Figure S6 Overview plot displaying the shape of all toluene and density depth profiles, grouped by SIC.** Panel labels
897 indicate the SIC bin. The scale bars for toluene and density in panel (A) apply also to panels (B) and (C).
898
899
900
901
902

Table S1.

Table S1 Fluxes and saturations calculated for the Arctic deployment using higher air mole fractions as modelled by Cabrera-Perez et al. (*25*)**.** For this calculation, all other parameters were kept the same and only the air mole fractions were increased to the values indicated in the table.

	benzene	toluene
Air mole fraction (pmol mol^{-1})	50	30
Saturation (%)	159	311
Flux (µmol m^{-2} d^{-1})	0.011	0.025

Table S1 shows that using higher air mole fractions in the Arctic does not change the conclusion of oceanic outgassing of benzene and toluene in the Arctic. Using higher air mole fractions, decreases the estimated benzene saturation by 74 % and the flux by 52 %. Similarly, using higher toluene mole fractions decreases the saturation by 87 % and the flux by 26 %. This calculation gives an appreciation of the potential uncertainty of the fluxes reported for the Arctic deployment due to the choice in air mole fraction.

Table S2.

Table S2 CAM-Chem simulation cases

Cases	Oceanic emission of Benzene in Polar regions	Oceanic emission of Toluene in Polar regions
noBT	-	-
avgBT	Arctic, >60ºN: 0.0244 μmol m^{-2} d^{-1} Antarctic, <-55ºS: 0.0236 μmol m^{-2} d^{-1}	Arctic, >60ºN: 0.0341 μmol m^{-2} d^{-1} Antarctic, <-55ºS: 0.0390 μmol m^{-2} d^{-1}
maxBT	Arctic, >60ºN: 0.158 μmol m^{-2} d^{-1} Antarctic, <-55ºS: 0.358 μmol m^{-2} d^{-1}	Arctic, >60ºN: 0.268 μmol m^{-2} d^{-1} Antarctic, <-55ºS: 0.158 μmol m^{-2} d^{-1}